

Bauhaus University Weimar
Faculty of Civil Engineering
Chair of Modeling and Simulation of Structures

**Aerodynamic Analysis Of Slender Vertical
Structures And Response Control Using
Tuned Mass Dampers**

by

Batta Septo Van Bahtiar Damanik

A thesis submitted in partial fulfillment of the requirements for the degree of
Master of Science
October 2015

DECLARATION

I hereby declare that all information in this document has been obtained and presented in accordance with academic rules and ethical conduct. I also declare that, as required by these rules and conduct, I have fully cited, referenced and duly acknowledged all material and results that are not original to this work.

Name: Batta Septo Van Bahtiar Damanik

Signature: _____

Date and place: October 10, 2015, Weimar.

ACKNOWLEDGEMENTS

I would like to thank Prof. Dr. Guido Morgenthal as my first supervisor for the chance to write my thesis under his supervision. It is such an honor to work the thesis and receiving feedback directly from him.

I would like also to thank my second supervisor, Mr. Dario Milani, to always patiently supervise and gives continuous support throughout the time of my thesis writing process.

I would like to say thank Mr. Samir Chawdhury and Mr. Khaled Ibrahim for the technical support in software operating and also for the non-technical support regarding computer pool access.

I also do not forget the financial support that I obtain for the past two years by DAAD (Deutscher Akademischer Austauschdienst) and without this support it is impossible for me to study and finish my master degree in Bauhaus University Weimar.

Last but not least, I would like to say thanks for all my family and friends for the moral support and for always being there and free their time for me especially in my weakest point.

Abstract

Analysis of vortex induced vibration has gained more interest in practical field of civil engineering. The phenomenon often occurs in long and slender vertical structure like high rise building, tower, chimney or bridge pylon, which resulting in unfavorable responses and might lead to the collapse of the structures. The phenomenon appears when frequency of vortex shedding produced in the wake area of body meet the natural frequency of the structure. Even though this phenomenon does not necessarily generate a divergent amplitude response, the structure still may fail due to fatigue damage. To reduce the effect of vortex induced vibration, engineers widely use passive vibration response control system. In this case, the thesis studies the effect of tuned mass damper. The objective of this thesis is to simulate the effect of tuned mass damper in reducing unfavorable responses due to vortex induced vibration and initiated by numerical model validation with respect to wind tunnel test report. The reference structure that being used inside the thesis is Stonecutter Bridge, Hongkong.

A numerical solver for computational fluid dynamics named *VXflow* which developed by Morgenthal [6] is utilized for wind and structure simulation. The comparison between numerical model and wind tunnel result shows 10% maximum tip displacement difference in the model of full erection freestanding tower. The tuned mass damper (TMD) model itself built separately in finite element software *SOFiSTiK*, and the effective damping obtained from this model then applied inside input modal data of *VXflow* simulation. A single TMD with mass ratio of TMD 0.5% to the mass of first bending frequency, the maximum tip displacement is measured to be average 67% reduced.

Considering construction limitation and robustness of TMD, the effects of multiple TMD inside a structure are also studied. An uncoupled procedure of applying aeroelastic loads obtained from *VXflow* inside finite element software *SOFiSTiK* is also done to observe the optimum distribution and optimum mass ratio of multiple tuned mass damper. The rest of the properties of TMD are calculated with Den Hartog's formula. The results are as follows: peak displacement in the case of multiple TMD that distributed with polynomial spacing achieve 7.8% more reduction performance than the one that distributed with equal spacing. Optimum mass of tuned mass damper achieved with ratio 1.25% mass of first bending frequency corresponds to across wind direction.

TABLE OF CONTENTS

Abstract	iii
List of Tables	v
List of Figures	vi
Chapter 1 Introduction	1
1.1 General Background	1
1.2 Objectives	2
1.3 Organization of Thesis	3
Chapter 2 Theoretical Background	4
2.1 Flow Past Bluff Body	4
2.2 Flow Around Circular Cylinder	6
2.3 Vortex Shedding	9
2.4 Structural Dynamics	11
2.5 Passive Vibration Control with TMD	14
Chapter 3 Study Case of Vortex Induced Vibration in Slender Structure 18	
3.1 Reference Object	19
3.2 Wind Tunnel Test	20
3.2.1 Vortex Shedding Responses	21
3.3 Numerical Simulation	22
3.3.1 Numerical Model of Tower with finite Element Software	22
3.3.2 Wind-Structure Numerical Simulation	25
3.4 Result and Comparison with Wind Tunnel Test	29
Chapter 4 Application of Tuned Mass Damper (TMD)	31
4.1 Design of TMD	31
4.2 Finite Element Modeling of the TMD	32
4.3 Numerical Simulation of TMD with VXflow	34
4.4 Numerical Simulation of TMD with FE Software	37
4.4.1 Wind-Structure Simulation	38
4.4.2 Parametric Simulation TMD	40
Chapter 5 Conclusion	48
5.1 Summary	48
5.2 Conclusion	49
5.3 Recommendation for Future Work	50
References	51
Appendices	53
Appendix A Input for VXflow	54
Appendix B Sofistik Code for TMD Calculation	59

LIST OF TABLES

Table 2.1	Classification of flow phenomena in circular cylinder, [9].	8
Table 3.1	Vortex shedding resonant responses, (without erection equipment).	22
Table 3.2	Dynamic responses definition of worst case wind angles.	22
Table 3.3	Eigenfrequency and modal mass of tower Stonecutter bridge.	26
Table 3.4	Comparison between Wind Tunnel (WT) and Numerical Simulation (NS).	30
Table 4.1	Reduction of maximum displacement (mm) in different elevation.	36
Table 4.2	Property of TMD.	42
Table 4.3	Comparison of tower respons: without, with 1 TMD, with 5 TMD.	42
Table 4.4	Coordinates of different schemes of multiple TMD distribution.	44
Table 4.5	Comparison of tower respons: Distribution of TMD.	44
Table 4.6	List of Mass Ratio Properties used in Simulation.	46
Table 4.7	Maximum displacement in variation of mass ratio.	46

LIST OF FIGURES

Figure 2.1	Flow of uniform stream past a bluff body.	5
Figure 2.2	Karman vortex street.	9
Figure 2.3	Across flow oscillation: before lock-in, lock-in, and after lock-in, after [15].	11
Figure 2.4	Illustration of single degree of freedom, redrawn after Zabel [13].	12
Figure 2.5	Principle of mass and stiffness proportional of Rayleigh damping,[13].	13
Figure 2.6	Decaying response curve of damped free vibration,[13].	14
Figure 2.7	Illustration of of main system (m) and pendulum (d) altogether,[13].	14
Figure 2.8	Freebody diagram of main system (m) and pendulum (d),[13]. .	15
Figure 3.1	Configuration of Stonecutter bridge, redrawn from Morgenthal, et al. [11].	19
Figure 3.2	Tower configuration, redrawn from Morgenthal, et al. [11]. . . .	20
Figure 3.3	Wind tunnel test model with erection height 293 m, [4].	21
Figure 3.4	Numerical model with Finite Element Software.	23
Figure 3.5	Comparison of eigenfrequency of tower in various erection stage.	24
Figure 3.6	Mode shapes (SOFiSTiK) of fully erected tower.	27
Figure 3.7	Tower input of slices and geometry for VXflow.	27
Figure 3.8	Multi slices dynamic pseudo 3D VXflow simulation.	28
Figure 3.9	Forces signal which meet the first bending frequency in the direction of vortex induced vibration.	28
Figure 3.10	Result of displacement time series at the top of tower.	29
Figure 3.11	Power spectral density (PSD) of tip displacement in 3 different erection stages.	30
Figure 4.1	Model consists of a sdof with a TMD system in SOFiSTiK. . . .	32
Figure 4.2	Comparison of dynamic amplification function in two-dof system.	33
Figure 4.3	Tuned mass damper inside tower.	34
Figure 4.4	Tower with tuned mass damper model in SOFiSTiK.	35
Figure 4.5	Decaying displacement response time histories of the tower with single TMD.	36
Figure 4.6	Comparison of displacement time histories.	37
Figure 4.7	Comparison of displacement time histories between VXflow, Sofistik, and Wind Tunnel.	39
Figure 4.8	Comparison of displacement responses of tower with TMD model.	41
Figure 4.9	Comparison of responses between structure: without TMD, with 1 TMD, with 5 TMD.	43
Figure 4.10	Multiple tuned mass damper model illustration.	43
Figure 4.11	Comparison of tip response with distribution case.	45
Figure 4.12	Reduction ratio of maximum tip displacement and acceleration.	47

Chapter 1

Introduction

1.1 General Background

Long and slender vertical structure often face problem due to wind action. Wind gusts confront the structures and within certain properties and characteristics of fluid-structure interaction, wind drives unfavorable responses to the structure. In the past many bridges have been damaged due to wind, but it was the collapse of the first Tacoma Narrows Bridge in 1940 that promoted bridge engineers worldwide to realize the consequences of wind induced excitation and to start the research on *aeroelastic* and *aerodynamic* actions of the wind. Aeroelastic and aerodynamic phenomena are two kinds of phenomena that cause vibration or even damage because of wind excitation. To distinguish between aeroelastic and aerodynamic phenomena, Kiviluoma explains the following [7]. Aeroelastic is the discipline concerned of significant interaction between aerodynamic forces and structural motions which often creates self excited forces. For body at rest, aeroelastic actions should vanish. Vortex induced vibration, flutter, galloping belongs to aeroelastic phenomenon while buffeting and turbulence induced vibration is treated as aerodynamic ones.

In a certain discrete wind regime, the frequency of vortex shedding may approach with one of the natural frequency of the structure. Such coincidence occur in self excited vibrations of the model. At finite range of wind speed beyond the resonance condition, the oscillation of the structure and not the wind speed controls the vortex shedding. In general, this lock-in phenomenon can cause the maximum amplitude to occur in higher wind speeds than expected by the resonance condition. This phenomenon named as *vortex induced vibration*. Due to this fact, engineer has to avoid the coincidence of Strouhal's frequency and structure's natural frequency.

Meanwhile, buffeting is defined as the unsteady loading of the structure by velocity fluctuations of the oncoming flow [3]. Structure like slender towers or decks exhibits aeroelastic interaction with the wind forces. Since the random buffeting load action on a structure may be viewed as a superposition of basic harmonic loads, the vibrations of

the structure may correspondingly be viewed as a superposition of harmonic responses induced by these loads. This phenomenon is named buffeting and it decreases the serviceability of the structure and could cause fatigue failure.

Two main types of device which are employed for the reduction of slender structure vibrations in translation and/or torsion are tuned mass dampers and viscoelastic dampers. Damping system of interest in the thesis is tuned mass dampers (TMD). Tuned mass dampers consist of a mass, usually of the order of 0.5% to 2% of the total mass of the structure, that is added to and interacts dynamically with the structure. Inherent in or attached to that mass is a system that dissipates energy during the relative mass-structure motion. Tuned mass damper control vibrations of tall and slender structure to withstand both wind and earthquake loads [3]. This TMD system is applied for the reference structure of the thesis, a bridge pylon of Stonecutter Bridge, in order to reduce huge vibrations occurred due to wind induced dynamic actions.

1.2 Objectives

The focus of this thesis is the study and the enhancement of a structural response that is controlled through the usage of TMD. The three main aspects involved within the achievements of the main goal are:

1. Description of wind induced excitation phenomena in the reference structure (a bridge pylon) and its relation to wind and dynamic properties such as turbulence, Reynolds numbers, natural frequencies, and modal parameters.
2. Numerical modeling of the structure. Numerical modeling of the CFD problem. Simulation of the coupled fluid-structure interaction problem.
3. Detailed study of response quantities such as displacements and internal forces.
4. Introduction and theory of optimization of the Tuned Mass Dampers which are attached to the reference structure in order to minimize unfavorable response such as large displacements or bending moments.

In order to achieve those four goals, a specific work flow of the thesis is structured as follows:

1. Literature review of the aerodynamic behavior of a circular cylinder, wind tunnel test of reference structure (Bridge Pylon), and fundamentals of Tuned Mass Damper.
2. Reference structure modeling with finite element software SOFiSTiK and SAP2000.
3. Wind modeling and structural pseudo 3D fluid-structure interaction using the Computational Fluid Dynamic solver VXflow.

4. Comparison with wind-tunnel reference results and calibration of the model.
5. Introduction of Multiple Tuned Mass Damper with correspondent optimization with respect to different parameters for sensitivity study such as damping ratio, mass ratio, frequency band ratio, and number of TMD.
6. The optimization strategy should be formalized into a Matlab script.
7. Application of Multiple Tuned Mass Damper on the reference structure and comparisons of responses to VIV of the structure with and without TMD respectively.
8. Proposal of the optimum scheme of Tuned Mass Damper to be built on the analyzed test case.

1.3 Organization of Thesis

The Thesis is composed of five chapters along with references and appendices at the end.

Chapter 1 comprises an introduction, objectives, and organization of the thesis

Chapter 2 contains a literature review of aerodynamic modeling and behavior of circular cylinder. It also contains structural dynamics and elaboration of tuned mass damper as vibration control system.

Chapter 3 explains the wind tunnel test report of reference structure along with the results obtained. In addition, a method of using computational fluid dynamics simulation using VXflow solver is also describe. VXflow's result and heir comparison with wind tunnel tests are elaborated in this chapter.

Chapter 4 presents numerical simulations of the reference structure with embedded tuned mass damper. Tuned Mass Damper is modeled using finite element software.

Chapter 5 depicts the conclusion and recommendation for future work.

Chapter 2

Theoretical Background

2.1 Flow Past Bluff Body

The motions of Newtonian viscous fluid for incompressible flow is described Navier Stokes equation [2].

$$\nabla \cdot \mathbf{u} = 0, \quad (2.1a)$$

$$\rho \frac{D\mathbf{u}}{Dt} = \rho \mathbf{g} - \nabla p + \mu \nabla^2 \mathbf{u}, \quad (2.1b)$$

where ρ is fluid density, \mathbf{u} is the velocity vector with component (u, v, w) , p is the pressure, g is gravity and μ is the viscosity. The symbol for ∇^2 is shorthand for

$$\frac{\partial^2}{\partial x^2} + \frac{\partial^2}{\partial y^2} + \frac{\partial^2}{\partial z^2}. \quad (2.2)$$

Recall that equation 2.1a represents conservation of mass and that left side of equation 2.1b represents the mass acceleration, or *inertia* terms in the equation, while the three terms on the right side are respectively the *body force*, the *pressure gradient*, and the *viscous term*. The term *body force* which contains gravity then could be annihilated due to very small external forces.

A body with length scale L (Figure 2.1) located in a fluid field which far away has constant uniform velocity U_∞ in x direction. The boundary condition of the velocity vector \mathbf{u} are $u = v = w = 0$ on the body surface S and $u \rightarrow U_\infty = v \rightarrow 0 = w \rightarrow 0$ at infinity. For a body given shape, the details of the flow will depend on U_∞ , L , fluid density ρ , and viscosity μ as well as on the shape of the body. The flow in fact only depends on one dimensionless parameter, the Reynolds number:

$$Re = \frac{\rho L U_\infty}{\mu}. \quad (2.3)$$

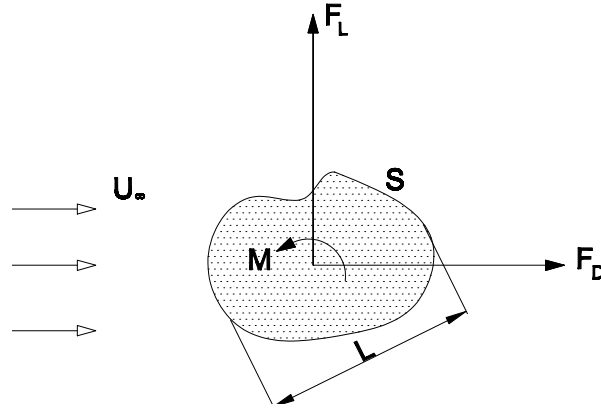


Figure 2.1: Flow of uniform stream past a bluff body.

Reynolds number is defined as the ratio between the inertial forces and the viscous ones. When Re is large, inertial effects predominate; when it is small, the viscous effects are the stronger ones.

Flows of practical interest have Reynolds numbers ranging from nearly zero to as high as 10^8 or 10^9 . Steadily increasing the Reynolds number of the flow over an obstacle generally produces a widely varying sequence of flow phenomena. At some point, flow over a body will separate and the wake will contain the effect of vortex formation. This formation of vortex was first reported by Strouhal and pointed out that the vortex-shedding phenomenon is describable in terms of a nondimensional number (the *Strouhal number*):

$$Sr = \frac{n_s L}{U}, \quad (2.4)$$

with n_s is frequency of vortex shedding from bluff objective of cross sectional dimension L . The drag, lift and moment on the body shown in Figure 2.1 proves to be of the form:

$$F_D = \frac{1}{2} \rho C_D L U^2, \quad (2.5)$$

$$F_L = \frac{1}{2} \rho C_L L U^2, \quad (2.6)$$

$$M = \frac{1}{2} \rho C_M L^2 U^2, \quad (2.7)$$

where U is the velocity of the wind, ρ the density of the air, C_D and C_L the drag and lift coefficient, C_M the moment coefficient and L the characteristic length of the object, such as projected length to the normal flow.

According to Davenport [8], there are three sources of aerodynamic excitations of wind causing the dynamic responses:

- forces induced by turbulent fluctuations in the oncoming onflow causing both

background and resonant responses in the along-wind and cross wind directions;

- forces induced by vortices shed in the wake of the structure; these affect primarily the resonant responses and occur primarily in the cross-wind direction;
- forced induced by motion of the structure; the most significant of these aerodynamic damping forces which control the resonant response amplitude. These can add to or subtract from the available structural damping. Negative aerodynamic damping is primarily associated with the cross-wind motion and can cause large amplitude oscillation and in the extreme case lead to aerodynamic instability.

The main phenomenon which studied in this thesis is the aerodynamic excitation that occurs due to shed of vortices in the wake of bluff body, or usually named as vortex induced vibration.

There are some approaches available to structural engineer to evaluate these dynamic responses. One of them is wind tunnel test which model the wind and structure with regarding significant dynamic and aerodynamic properties of the natural wind and the structure modeled. The response of the scale structure is directly inferred from measurements of the model. In wind tunnel test, one requires understanding of the scaling laws. Beside Reynolds number which takes into account the viscosity there is also *Froude number* which consider the inertial and gravitational force. Froude number is described in:

$$Fr = \frac{U^2}{Lg}, \quad (2.8)$$

with U is velocity of wind, L is characteristic length, and g is gravity and it constitutes the main reference for wind tunnel scaling. Both Reynolds number and Strouhal number are dimensionless numbers which play roles in wind tunnel similitude, particularly in aiding the transfer of results from experimental model to full-scale prototype.

2.2 Flow Around Circular Cylinder

Circular cylinder belong to a class of bodies which may be termed semi-aerodynamic, as compared to aerodynamic bodies such as aerofoils, and non-aerodynamic bodies with sharp edges such as squares [9]. Aerodynamic bodies avoid separation, non-aerodynamic bodies have fixed separations at some of the corners. With semi-aerodynamic bodies the position of separation is varying depending on free stream velocity and flow profile, free stream turbulence, geometry, and the roughness of the body's surface.


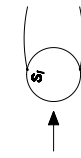
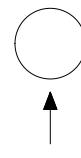

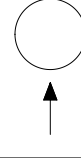
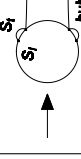

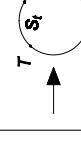
The flow of incompressible fluid around a circular cylinder is one of the most challenging problems in aerodynamics, considering both theory and physical phenomena. The

classical works were contributed by Thodore von Karman (1912) regarding the vortex street, Taylor (1915), Wieselsberger (1921) dealing with the variation of the drag cylinders with smooth surface and the influence of aspect ratio, and Fage and Warsap (1930) investigating the effect of free stream turbulence and surface roughness on the drag and on the pressure distribution. This classical method requires big computational effort to be implemented in numerical simulation. Because in order to find the exact point of separation in the cylinder, one must create big number of discretisation. Amount of computational cost rises with factor of power two with respect to number of discretisation of the body [5].

The flow around circular cylinder depends on Reynolds number Re , since the state of the boundary layer may be either laminar or partly turbulent. In turbulent conditions, additional energy is fed to the boundary layer by turbulent momentum exchange and hence it gains additional capability of overcoming the adverse pressure gradient behind the pressure minimum, producing a smaller width of the wake, recovery of the wake pressure and smaller drag. Various phenomena of the different stages of transition from subcritical to transcritical have been clarified by Schewe (1983) [10]. Schewe's result is condensed in Table 2.1.

1. The boundary between subcritical and critical range has been chosen by Schewe as the onset of randomization of lift fluctuation, obvious in the spectral density function (SDF) of lift and occurring at $Re = 2.8 \cdot 10^5$. Below this boundary, there is regular vortex shedding at a Strouhal number of $Sr = 0.2$. This is a rather sharp, well defined boundary.
2. The critical regime are from $Re = 1.4 \cdot 10^5$ up to $Re = 3.5 \cdot 10^6$ (ranges (2) to (5) in Table 2.1), where Re_{crit} is rather well defined by the drag minimum. Schewe's detailed analysis of the fine structure of the critical range reveals four different states of the flow. In Table 2.1, there is an intermediate, unsymmetrical configuration (4) where the separation bubble forms on one side of circumference only. This pattern is called bistable because the one-sided bubble may occur on either side. Preceding is an unstable situation (3) where the boundary layer jumps between laminar and turbulent separation leading to random lift fluctuation. A second unstable range (5) follows the bistable, until separation bubbles occur in both sides at Re_{crit} .
3. The supercritical regime is at first stable (6) with two separation bubbles and narrow band lift fluctuations with $Sr = 0.48$ the highest value observed. The following upper transition range (7) marks the transition into transcritical regime. The separation bubble disappears, and the transition point T from laminar to turbulent state of flow in the boundary layer shifted upstream as Re increases. The boundary between super and transcritical is defined by the situation, when the transition points T and the turbulent separation points S_t have reached more or less constant positions, Achenbach [1971], at $Re \approx 5 \cdot 10^6$.

Table 2.1: Classification of flow phenomena in circular cylinder, [9].

	subcritical		critical				supercritical		transcritical
	(1)	(2)	(3)	(4)	(5)	(6)	(7)	(8)	
state of boundary layer	stable		unstable	bistable	unstable	stable	unstable	stable	
10^5 Re		1.4 - 2.8	2.8 - 3.0	3.0 - 3.3	3.3 - 3.5	3.5 - 10	10 - 50	> 50	
mean drag C_d	1.2	1.2 - 1.0	1.0 - 0.7	0.5	0.5 - 0.4	0.22	0.22 - 0.52	0.52	
mean lift C_l		0		± 1.3	1.3 - 0.9	0	0.1 - 0.2	0	
Fluctuating lift SDF	single narrow peak		random with two peaks	narrow peak	random peak	narrow peak	random with two broad peak	rather narrow peak	
Sr		0.2	0.2	0.33	0.31	0.48	0.1/0.45	0.28	
$C_{l,rms}$		0.25 - 0.09	0.09 - 0.06	0.04	0.04 - 0.07	0.02	0.04	0.05	
boundary layer separation	laminar S_l								
									
	laminar S_l	laminar	random	one sided bubble	random	two sided bubble	random	turbulent	

2.3 Vortex Shedding

The shedding of vortices behind bluff bodies, and particularly from two dimensional circular cylinders, is perhaps one of the most studied subjects in fluid dynamics. The person who first stimulated the vortex shedding phenomenon is Theodore von Karman, with his article published in Göttingen in 1911 and 1912. In his honor the double row of vortices of opposite sign shed from a cylinder become rapidly known as *Karman vortex street* [14].

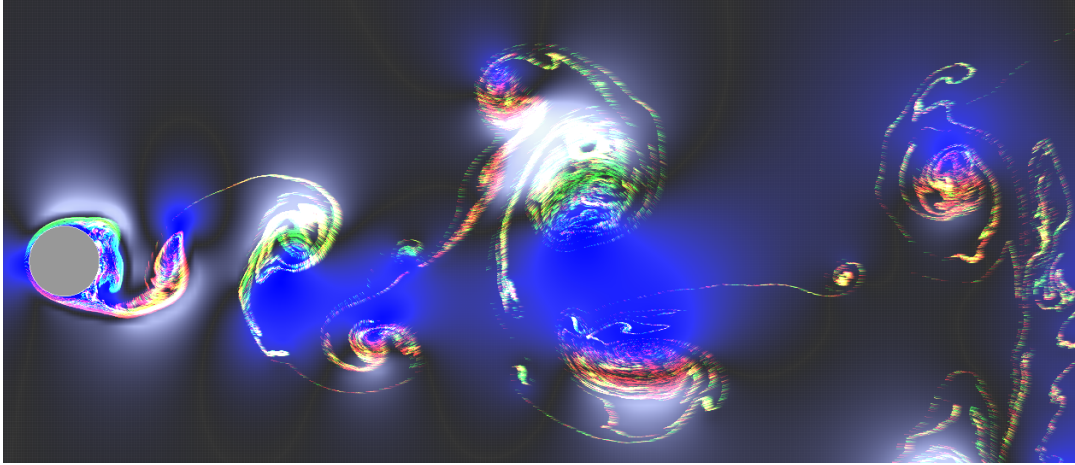


Figure 2.2: Karman vortex street.

Karman decided to make crude estimation of the stability of the vortex within two parallel rows of ideal inviscid vortices of opposite sign, and find that the configuration was always unstable except for a particular antisymmetrical configuration having a critical ratio l/h , where l is the distance between consecutive vortices and h the separation between the two rows, which is $l/h \cong 0.2806$.

Force acting on bluff bodies as a consequence of vortex shedding may lead into significant and potentially dangerous self excited excitations. In order to investigate this phenomenon, engineers started the research by studying the stability of the wake and by evaluating the vorticity in two dimensional bluff body flows. These studies had been applying the theoretical stability analysis and the concepts of absolute and convective instability to determine the velocity profile in the wakes of bluff body, thus measured frequencies of vortex shedding.

The process when a vortex may be considered to be completely shed from the body, and a new one of the same sign to start its formation process, is not yet as clear as one might presently hope. The importance of understanding the essential physics of this process is due to the fact that, in any attempt of devising a simplified model of vortex shedding, it should correctly be taken into account in order to obtain reasonable estimates of the shedding frequency.

Numerical Method for Vortex Shedding Simulation

The numerical prediction of vortex shedding from two dimensional bluff bodies and of the related mean and fluctuating forces has always been a challenging subject of research. One of the idea to reach a simplified model but still describing properly its fundamental physical features is *discrete vortex methods*. This method reviewed by Clements (1973), Clements and Maull (1975), Sarpkaya (1975), Stansby (1977), Sarpkaya and Shoaff (1979), and Stansby (1985). In these methods, the continuous sheets of vorticity shed from the separation points are discretized by means of ideal point vortices (which are actually the cross section of line vortices), containing the vorticity shed in a certain time interval Δt . These vortices are then convected by the velocity field, which is the result of freestream flow, the perturbation field produced by the presence of the body boundary, and the velocities induced by all the vorticities shed in previous time steps [14].

VXflow, a numerical solver developed by Morgenthal [6] applied similar vortex method inside its calculation algorithm. The method called as *vortex particle method*, which based on grid free Lagrangian formulation by Navier Stokes equation, where the velocity field is modeled by particles representing vorticity. These particles are being convected due to free stream velocity as well as diffused. This representation yields the main advantages of low numerical diffusion, compact discretization as the vorticity is strongly localized, implicitly accounting for the free space boundary conditions and natural representations of the vortex creation process inherent in bluff body flows [5]. The modeling of the wind flow inside this thesis uses the numerical solver of VXflow.

Vortex Induced Vibration

If the body that instigates the vortex shedding is elastically supported or if it is subject to local contour deformation, it will deflect wholly or locally and, by this action, influence the local flow. The circular cylinder will be driven periodically under the action of the vortex shedding in its wake, but this driving will evoke only small response unless the Strouhal frequency of alternating pressures approach the across flow natural frequency of the cylinder. Greater body movement is evoked near this frequency, and the body begins to interact strongly with the flow [3].

It is experimentally observed at this point that the body natural frequency controls the vortex shedding phenomenon even when variations in flow velocity displace the nominal Strouhal frequency away from natural frequency by few percent. This control of the phenomenon by mechanical forces is commonly known as lock in or synchronization. Observations show that during lock in the amplitude of the oscillations attains some fraction, rarely exceeding half, of the across-wind dimension of the body.

Among the many empirical analytic models of vortex induced oscillation, there are

some experiments that recognize the near sinusoidal response of the cylinder at each of two prominent frequencies, Strouhal and the natural frequency of the structure. Experiments after Goswami, et al [15] depict some illustrative result for deflection responses of an elastically supported circular cylinder before lock-in, at lock-in, and after lock-in, respectively, together with the corresponding displacement spectra, where f_s , f_n are the Strouhal and natural frequencies, respectively. The illustration is shown in Figure 2.3.

One particular aspect of vortex induced vibration is in the wake of the body produced a street of alternately shed vortices coupled in a fairly complex manner to the oscillation of the body. Another characteristic is that while self excited, it never proceeds to divergent amplitudes but enters a limit cycle of relatively modest level.

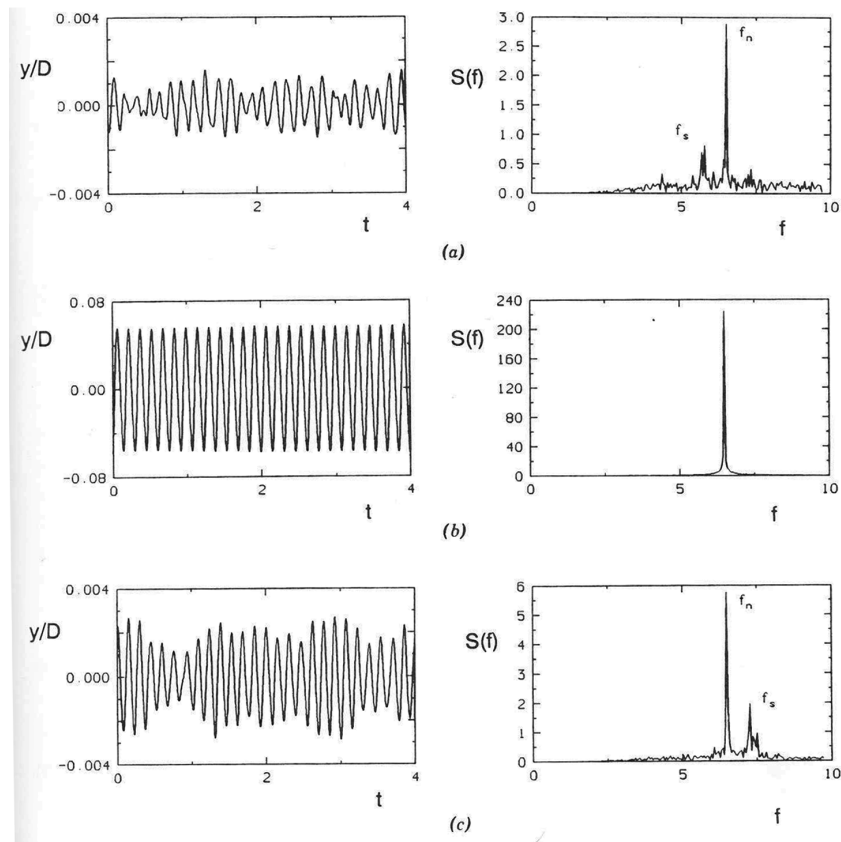


Figure 2.3: Across flow oscillation: before lock-in, lock-in, and after lock-in, after [15].

2.4 Structural Dynamics

In order to evaluate the behavior of structure under aerodynamic effects of wind, one must first understand the fundamental aspects of structural dynamics. Structural dynamics study the structural response due to time dependent loads, such as wind or earthquake. The basic form of structure is called single degree of freedom system, which

consists of a single mass m and can move in single direction with its deformability or stiffness (spring constant k) and an energy dissipation (damping constant c). Equation of motion describing motion of the mass described by the equation:

$$m\ddot{x} + c\dot{x} + kx = F(t). \quad (2.9)$$

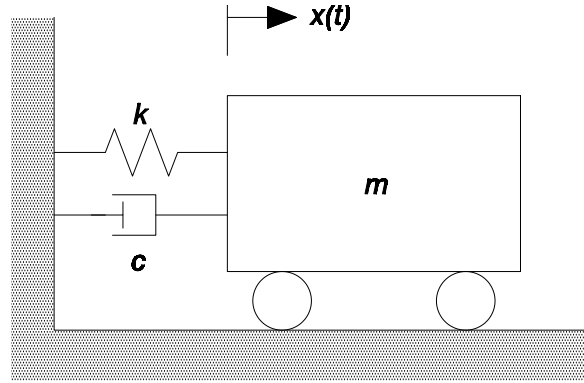


Figure 2.4: Illustration of single degree of freedom, redrawn after Zabel [13].

The damping of a sdof system is often described by the damping coefficient ζ which represent the ratio of damping to damping critical.

$$\zeta = \frac{c}{c_{crit}} = \frac{c}{2m\omega_0} \rightarrow c = 2m\omega_0\zeta. \quad (2.10)$$

When the forces $F(t)$ exist in a form of harmonic function $\hat{F} \sin \Omega t$, there are a formula to relate the effects of dynamics load into static load which usually called dynamic amplification factor (V):

$$V = \frac{\hat{x}}{x_{stat}} = \frac{1}{\sqrt{\left(1 - \frac{\Omega^2}{\omega_0^2}\right)^2 + \left(2\zeta \frac{\Omega}{\omega_0}\right)^2}}, \quad (2.11)$$

where Ω is the excitation frequency and ω_0 is natural frequency of the structure.

For the most practical case, multi degree of freedom required to be model to represent the system. Instead of using one single value, matrices of mass $[M]$, stiffness $[K]$, and damping $[C]$. The excitation force is also expressed in a form of vector $\{F\}$. Generally the equation of motion for multi degree of freedom is:

$$[M]\{\ddot{x}\} + [C]\{\dot{x}\} + [K]\{x\} = \{F\}. \quad (2.12)$$

The vectors $\{F\}$ and $\{x\}$ are of dimension n . $[M]$, $[K]$, and $[C]$ are positive (semi) definite matrices, they have no negative eigenvalues, of dimension $n \times n$. In certain cases, the construction of viscous damping matrix $[C]$ can be required. The simplest

way is to assume proportionality of the damping matrix to either stiffness or the mass matrix. This proportional damping is named as Rayleigh damping and expressed in both stiffness and mass proportional damping:

$$\zeta_k = \frac{1}{2} \left(\alpha \omega_k + \frac{\beta}{\omega_k} \right), \quad (2.13)$$

with ζ_k is modal damping ratio, α and β are the factors of stiffness and mass proportional damping respectively and ω_k is natural circular frequency.

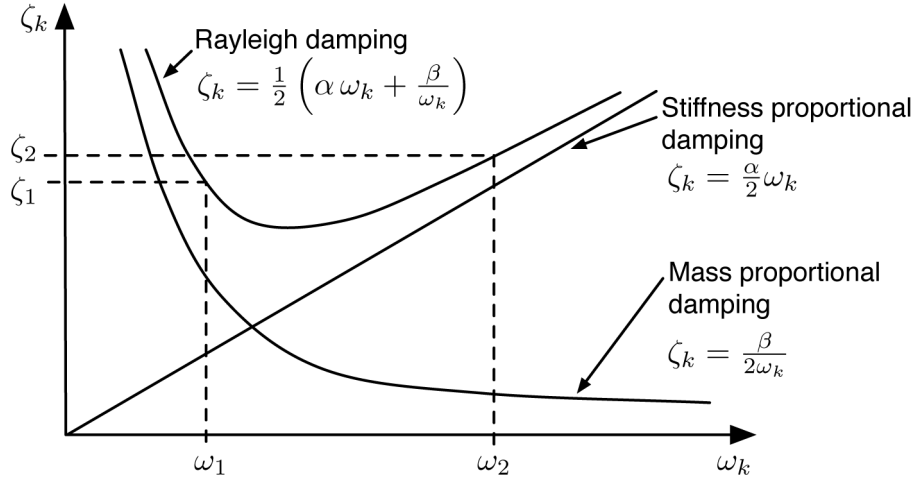


Figure 2.5: Principle of mass and stiffness proportional of Rayleigh damping,[13].

Logarithmic decrement is another tool to measure damping in a system from a time history. Logarithmic decrement is defined as the natural logarithm of any two successive amplitudes on the same side of the mean position in an under-damped system [24]. It is denoted by Λ . Actually the ratio of any two successive amplitudes in an under-damped system is always constant.

If we consider time instant t_1 and $t_1 + nT$ we have:

$$\Lambda = \frac{1}{n} \ln \frac{x(t_1)}{x(t_1 + nT)}, \quad (2.14)$$

$$\zeta = \frac{\Lambda}{\sqrt{4\pi^2 + \Lambda^2}}. \quad (2.15)$$

These two equations are used in the case of calculating damping from a measured displacement of free vibration over the time.

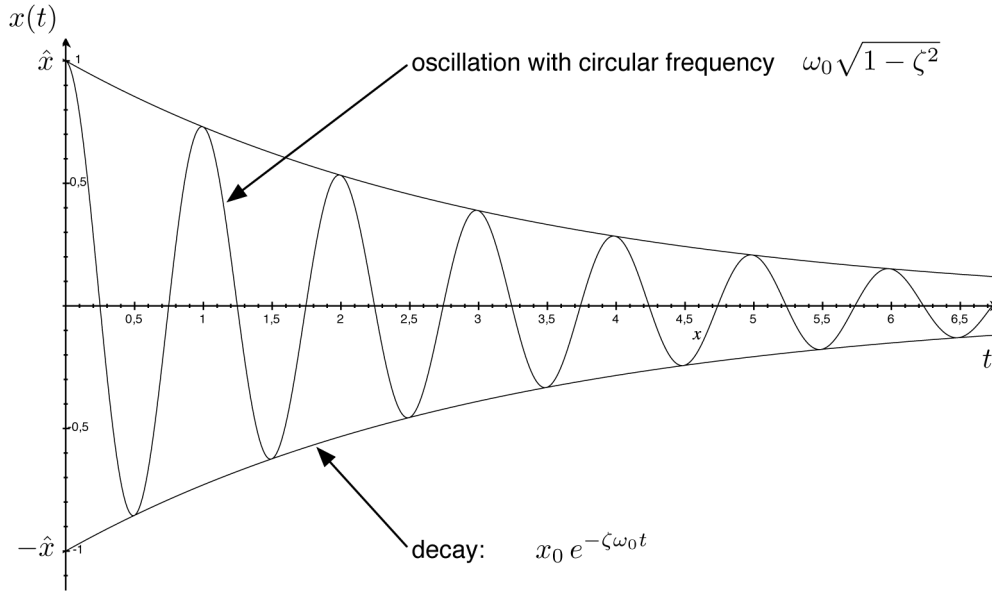


Figure 2.6: Decaying response curve of damped free vibration,[13].

2.5 Passive Vibration Control with TMD

Tuned mass damper (TMD) is a passive energy absorbing device consists of a mass, a spring, and a viscous damper attached to a vibration system to reduce unfavourable response. The tuned mass damper is usually modeled as swinging pendulum. The illustration of tuned mass damper in a single degree of freedom system given in Figure 2.7 and the force acting at the total system and at the pendulum subsystem are summarised in figure 2.8.

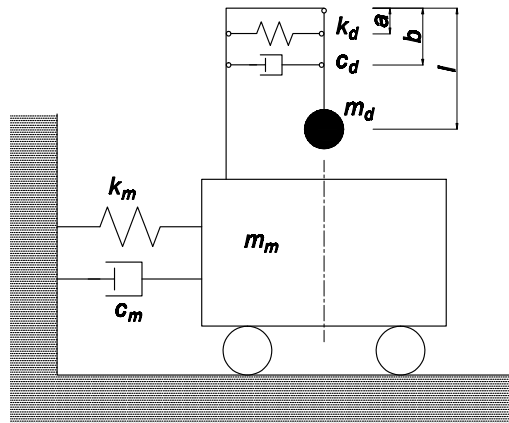
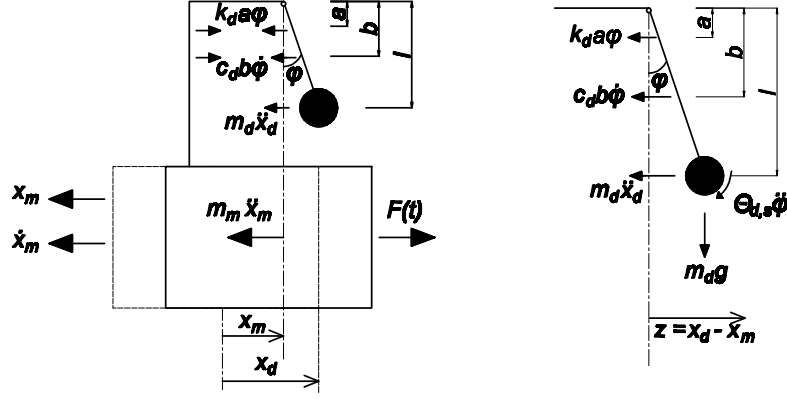


Figure 2.7: Illustration of of main system (m) and pendulum (d) altogether,[13].

Based on Figure 2.8 we can derive the equations of motion for both the total system


 Figure 2.8: Freebody diagram of main system (m) and pendulum (d), [13].

and the pendulum:

$$m_m \ddot{x}_m + m_d \ddot{x}_d + c_m \dot{x}_m + k_m x_m = F(t), \quad (2.16)$$

$$m_d \ddot{x}_d l + \Theta_{d,s} \ddot{\varphi} + c_d b^2 \dot{\varphi} + k_d a^2 \varphi + m_d g (x_d - x_m) = 0. \quad (2.17)$$

If we set now:

$$x = x_m, \quad z = x_d - x_m \quad \longrightarrow \quad x_d = z + x_m, \quad (2.18)$$

$$z = \varphi l \quad \longrightarrow \quad \varphi = \frac{z}{l} \quad \longrightarrow \quad a\varphi = \frac{a}{l}z; \quad b\varphi = \frac{b}{l}z, \quad (2.19)$$

equations 2.16 and 2.17 become:

$$(m_m + m_d) \ddot{x} + m_d \ddot{z} + c_m \dot{x} + k_m x = F(t), \quad (2.20)$$

$$m_d \ddot{x} + M_d \ddot{z} + C_d \dot{z} + K_d z = 0, \quad (2.21)$$

with

$$M_d = m_d + \frac{\Theta_{d,s}}{l^2}, \quad C_d = \frac{c_d b^2}{l^2}, \quad K_d = \frac{m_d g}{l} + \frac{k_d a^2}{l^2}. \quad (2.22)$$

The natural circular frequencies of the main system ω_m and of the damper ω_d defined

by:

$$\omega_m = \sqrt{\frac{k_m}{m_m}}, \quad \omega_d = \sqrt{\frac{K_d}{M_d}} = \sqrt{\frac{m_d g l + k_d a^2}{m_d l^2 + \Theta_{d,s}}}. \quad (2.23)$$

With the mass ratio $\mu = \frac{m_d}{m_m}$ and the relation $c = 2m\omega_0\zeta$ we obtain:

$$(1 + \mu)\ddot{x} + \mu\ddot{z} + 2\omega_m\zeta_m\dot{x} + \omega_m^2 x = \frac{F(t)}{m_m}, \quad (2.24)$$

and

$$\frac{m_d}{M_d}\ddot{x} + \ddot{z} + 2\omega_d\zeta_d\dot{z} + \omega_d^2 z = 0. \quad (2.25)$$

These equations of 2.24 and 2.25 are used to solve the system two degree of freedom and lead to the either displacement, velocity, or acceleration of the system.

If we want to solve the equation with case of harmonic excitation:

$$F(t) = \hat{F} \sin \omega t = \hat{F} e^{i\omega t}, \quad (2.26)$$

with ansatz functions:

$$x = \hat{x} e^{i\omega t}, \quad z = \hat{z} e^{i\omega t}, \quad (2.27a)$$

$$\dot{x} = i\omega \hat{x} e^{i\omega t}, \quad \dot{z} = i\omega \hat{z} e^{i\omega t}, \quad (2.27b)$$

$$\ddot{x} = -\omega^2 \hat{x} e^{i\omega t}, \quad \ddot{z} = -\omega^2 \hat{z} e^{i\omega t}, \quad (2.27c)$$

we have:

$$[-(1 + \mu)\omega^2 + i2\omega_m\zeta_m\omega + \omega_m^2]\hat{x} - \mu\omega^2\hat{z} = \frac{\hat{F}}{m_m}, \quad (2.28)$$

$$-\frac{m_d}{M_d}\omega^2\hat{x} + [-\omega^2 + i2\omega_d\zeta_d\omega + \omega_d^2]\hat{z}. \quad (2.29)$$

From these expression one can derive the following relation for the dynamic amplitude amplification of the main system:

$$V_1 = \frac{\hat{x}}{x_{stat}} = \sqrt{\frac{A^2 + B^2}{C^2 + D^2}}, \quad (2.30)$$

with

$$A = -\eta^2 + \kappa^2, \quad (2.31a)$$

$$B = 2\kappa\zeta_d\eta, \quad (2.31b)$$

$$C = [1 + (1 - \alpha)\mu]\eta^4 - [1 + 4\kappa\zeta_m\zeta_d + (1 + \mu)\kappa]\eta^2 + \kappa^2, \quad (2.31c)$$

$$D = -2[\zeta_m + (1 + \mu)\kappa\zeta_d]\eta^3 + 2\kappa(\kappa\zeta_m + \zeta_d)\eta, \quad (2.31d)$$

where

$$\kappa = \frac{\omega_d}{\omega_m}, \quad \eta = \frac{\omega}{\omega_m}, \quad \alpha = \frac{m_d}{M_d}, \quad (2.32)$$

According to Den Hartog, an optimum Tuned Mass Damper which reduce amplification response due to dynamic excitation is defined by with two parameters which are frequency ratio κ and and damping ratio of the damper ζ_d .

$$\kappa_{opt} = \frac{1}{1 + \mu}, \quad (2.33)$$

$$\zeta_{d,opt} = \frac{3\mu}{8(1 + \mu)^3}. \quad (2.34)$$

These two parameters of κ_{opt} and $\zeta_{d,opt}$ depends only on the mass ratio. The determination of TMD mass is significant regarding both the significance for reducing responses and the cost of TMD material.

Chapter 3

Study Case of Vortex Induced Vibration in Slender Structure

Slender structures with large aspect ratio are vulnerable to wind excitation, especially to the aeroelastic phenomenon in across wind direction of vortex induced vibration. High rise building, chimney, and also a bridge pylon are the several types of structures which often deal with this phenomenon. Although vortex induced vibration is occurred without divergent amplitude, it still would result in failure or loss of serviceability due to large structural response. As previously said in chapter 2, this self excited force comes from the shedding of vortices in the wake region of the body, and when the Strouhal's frequency synchronizes the natural frequency, the motion of the structure suddenly increase. This phenomenon called as lock-in or synchronization.

In this chapter numerical modeling of wind is simulated to obtain the vortex induced vibration phenomenon. Numerical solver used to analyze this computational fluid dynamic problem is VXflow which was firstly developed by Morgenthal [6]. Simulation to obtain dynamic characteristic of the reference structure itself is done with means of finite element softwares SOFiSTiK and SAP2000. The responses of the structure due to vortex induced vibration are then obtained through the forces acquired from VXflow and simulated in finite element software. A wind tunnel test report was performed in same manner of numerical simulation. Result comparisons between both of experimental and numerical analysis are later discussed.

In order to improve the performance of the structure, tuned mass damper system is introduced. The concept of tuned mass damper was established by Frahm [16] and this damping system is one of the most promising and effective passive vibration suppression devices. Tuned mass damper basically consist of a mass, a spring, and a viscous damper attached to a vibrating system. The application of tuned mass damper is elaborated later in chapter 4.

3.1 Reference Object

The bridge pylon or tower of Stonecutter Bridge is the reference object to be studied in the thesis. The Stonecutter Bridge itself built in Hong Kong with a high level cable stayed bridge and two towers located in the back-up areas of Container Terminals 8 and 9 respectively, and forms part of Route 9 between Tsing Yi and Chueng Sha Wan. The bridge has main span of 1018 m across the Rambler Channel and a total length, including the back spans, of approximately 1600. The bridge concept is characterized by a twin deck suspended from two single pole towers. These towers are 293 m high and of tapered circular cross section measuring 7 m at the top and 14 m at the deck level. Two thirds of the towers will be constructed in concrete and the top third will be of composite construction consisting of an inner concrete ring with a stainless steel skin [4].

Each tower has an average height to width ratio (aspect ratio) of 1:30 which considered as a tall and slender structure. The tower plays an important role for keeping the bridge sound and any disturbance due to wind excitation will immediately influence the traffic service condition of the bridge. In the next sections, the free standing tower is analysed thoroughly with both wind tunnel test and numerical simulation.

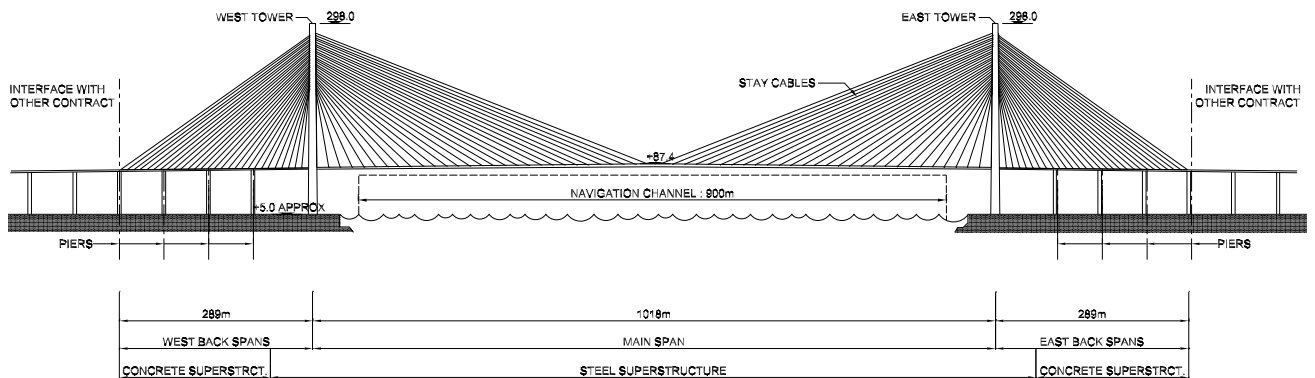


Figure 3.1: Configuration of Stonecutter bridge, redrawn from Morgenthal, et al. [11].

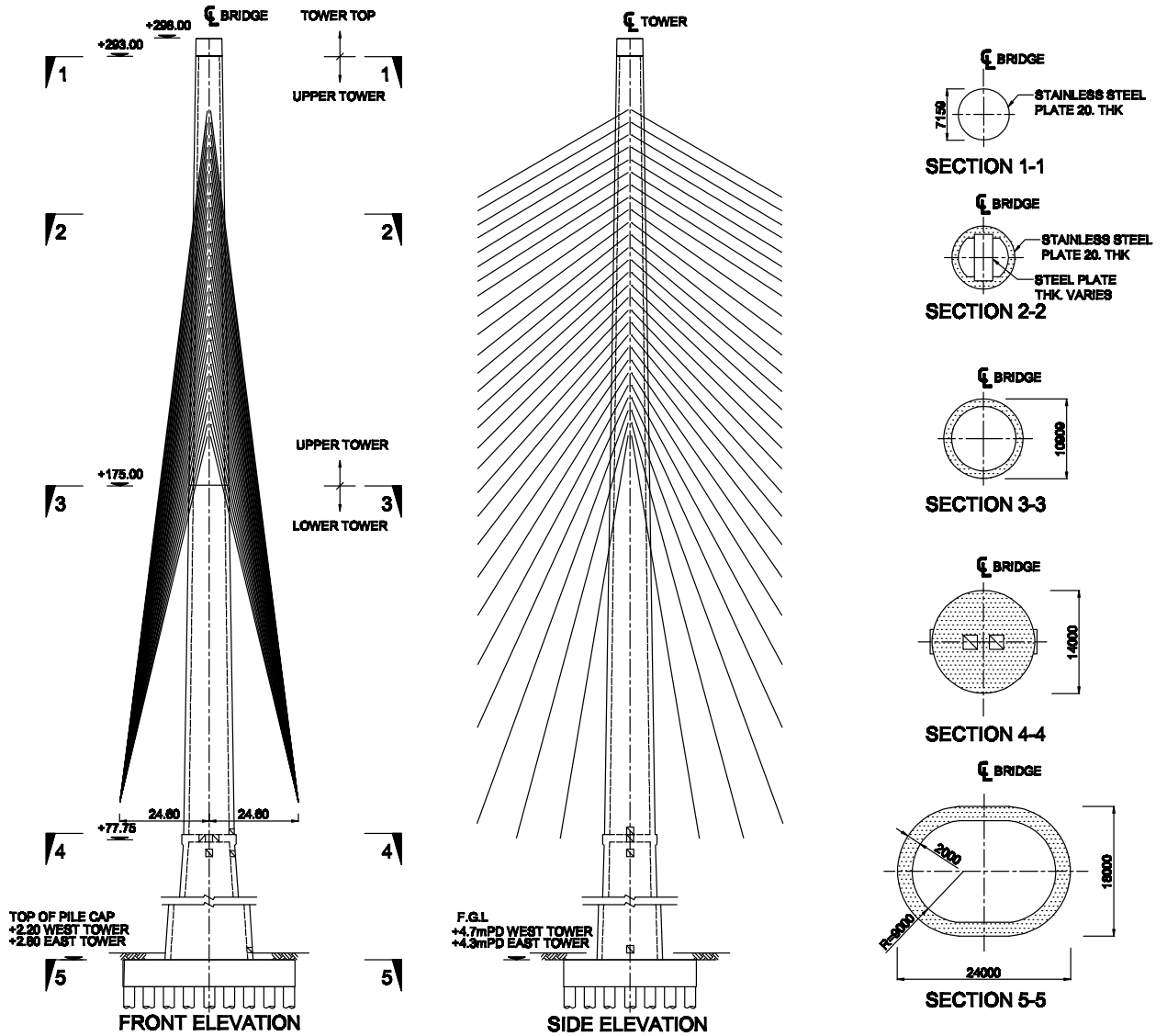


Figure 3.2: Tower configuration, redrawn from Morgenthal, et al. [11].

3.2 Wind Tunnel Test

BMT Fluid Mechanics Limited conducted a wind tunnel test of freestanding tower of Stonecutter Bridge. An instrumented tower of scale 1:200 was tested for purpose of conducting smooth flow and turbulent flow boundary layer. The test also takes into consideration of four erection heights of free standing tower and multiple levels of damping. To confirm the final detail of proposed turbulence simulation, they conducted a series of wind speed and spectral measurements using hot wire anemometry and tuned it based upon stated deck level targets for the turbulence conditions.

The tests measure tip motions at the top of the tower legs (along and perpendicular to the longitudinal axis) and damping level of 0.0125 log dec, with and without erection equipment. Freestanding tower without erection equipment will be the focal point of this study. Later, the comparison of each stages of erection are also elaborated for

purpose of affirmation with numerical simulation. A figure from the test is shown in Figure 3.3.

The assessment of four key erection stages are the construction phase of tower in heights of 119 m, 174 m, 246 m and 293 m. In addition, this test have assessed the aerodynamic interference effects of the temporary erection equipment anticipated for the respective construction stages on the mean wind loading and the vortex shedding response of the tower relevant to construction process.

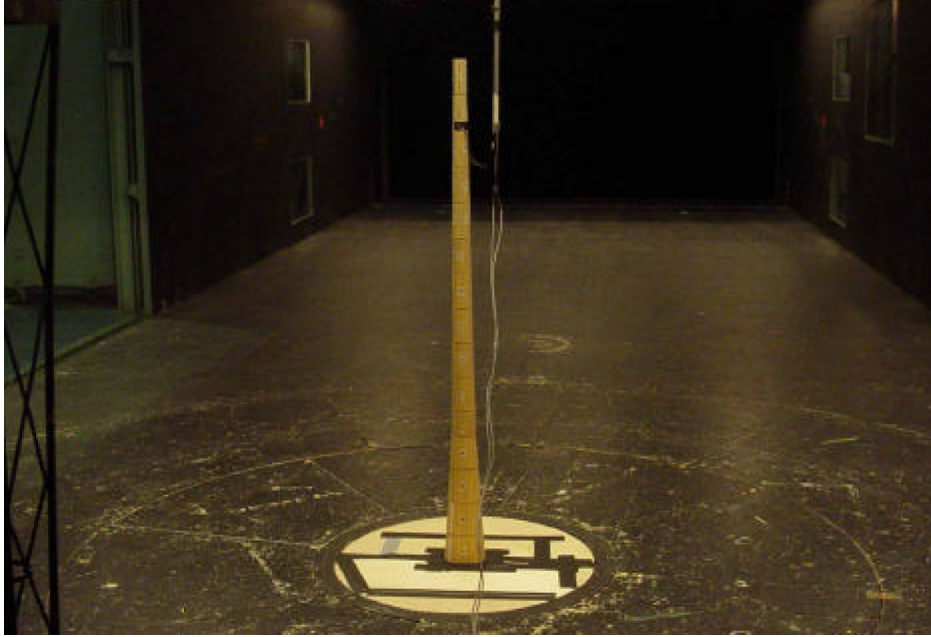


Figure 3.3: Wind tunnel test model with erection height 293 m, [4].

3.2.1 Vortex Shedding Responses

The Reynolds number at the vortex shedding was of the order of 10^4 at model scale corresponding to 10^7 at full scale. This discrepancy affects the vortex shedding critical wind speed as Strouhal number varies with Reynolds number. The fully erected tower exhibits vortex shedding resonance response in smooth flow at 9.5 m/s with Strouhal number 0.17, based on average diameter of top third section of tower. The fully erected tower exhibits a maximum vortex shedding resonant response in smooth flow (at 9.5 m/s wind speed) of approximately 150 mm for structural damping of 0.01 logdec. The highest vortex shedding resonant responses and corresponding wind speeds and wind angles are providing in Table 3.1 and 3.2.

Table 3.1: Vortex shedding resonant responses, (without erection equipment).

Erection Height (m)	Critical Wind Speed (m/s)	Max Displacement at Tip (mm)	Max Acceleration at Tip (m/s)	Structural Damping (logdec)
293	9.5	150	0.2	0.01
246	15-18	27	0.06	0.01
174	27.5	31	0.24	0.03
119	-	-	-	0.03

Table 3.2: Dynamic responses definition of worst case wind angles.

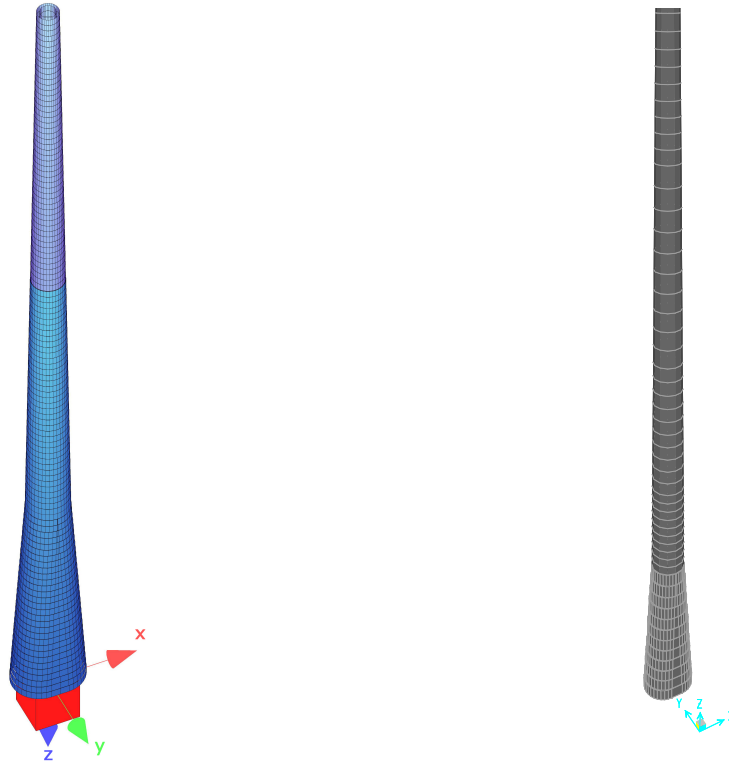
Erection Height (m)	Erection Equipment	Wind Angle Most Susceptible to Vortex Shedding Resonance (°)
Stage EH4 - 293m	without	1
Stage EH3 - 246m	without	8
Stage EH4 - 174m	without	4
Stage EH4 - 119m	without	1

3.3 Numerical Simulation

The tower has primarily circular section, except one fifth part at the bottom of the span, which has shape of rectangle with arch on its two sides and can be seen in Figure 3.2. The pylon is mostly made of concrete, only in top third of the tower it has additional stainless steel plate 20 mm thick, which cast together with concrete. In numerical model, the modification of concrete stiffness and mass in the top third of tower compromise this composite section, while this modification considered as uncomplicated procedure but still leads to accurate and relevant result. In the interest of wind tunnel test report, this numerical model satisfy the fundamental dynamics properties.

3.3.1 Numerical Model of Tower with finite Element Software

Finite element softwares used for modeling the structure of tower are SOFiSTiK and SAP2000. The tower modeled as a beam hollow cross section, with variation of radius and thickness along the span. The section material used is concrete with modulus of elasticity, $E = 28000$ MPa and unit weight of 25 kN/m³. For the top third of the section, the unit weight of the concrete is modified into 26 kN/m³ due to the added 20 mm stainless steel plate. The tapered geometry along the span was made by creating a group of section which has gradual change of dimension. In SOFiSTiK software, one can make use of simple mathematical loop to create this group of section but not in SAP2000. That is the reason why in Figure 3.4 the transition of section appeared smoother in SOFiSTiK model rather than in SAP2000 model. Modeling with



(a) Numerical model with SOFiSTiK.

(b) Numerical Model with SAP2000.

Figure 3.4: Numerical model with Finite Element Software.

at least two different numerical software is needed, that the result obtained from each simulation could be compared.

Dynamic properties acquired from the numerical simulation includes the following: natural/eigen frequencies, mode shapes, and mass participation factor of each modes. Since there are plausible dynamic properties of the tower available from wind tunnel test report, some adjustment and calibration in numerical model has been made to affiliate the result. Some adjustments accomplished are for instance the simulation of cracked and uncracked section and the trial and error of putting additional mass and stiffness due to added composite sections.

After series of calibrations and adjustments, the result is obtained. Figure 3.5 shows the comparison of first four modes acquired from SOFiSTiK and SAP2000 simulations in four key erection stages. However in the first two erection stages Figure 3.5a and 3.5b, the wind tunnel test report only present first and second mode but later in Figure 3.5c and 3.5e it provides the data of all four modes. The first and second modes of every erection stages shows relatively small discrepancy as to wind tunnel test report. On the other hand, the third and four modes collected from each simulation appeared with less correlation.

As the first step of simulation, this comparison is important to prove the validity of

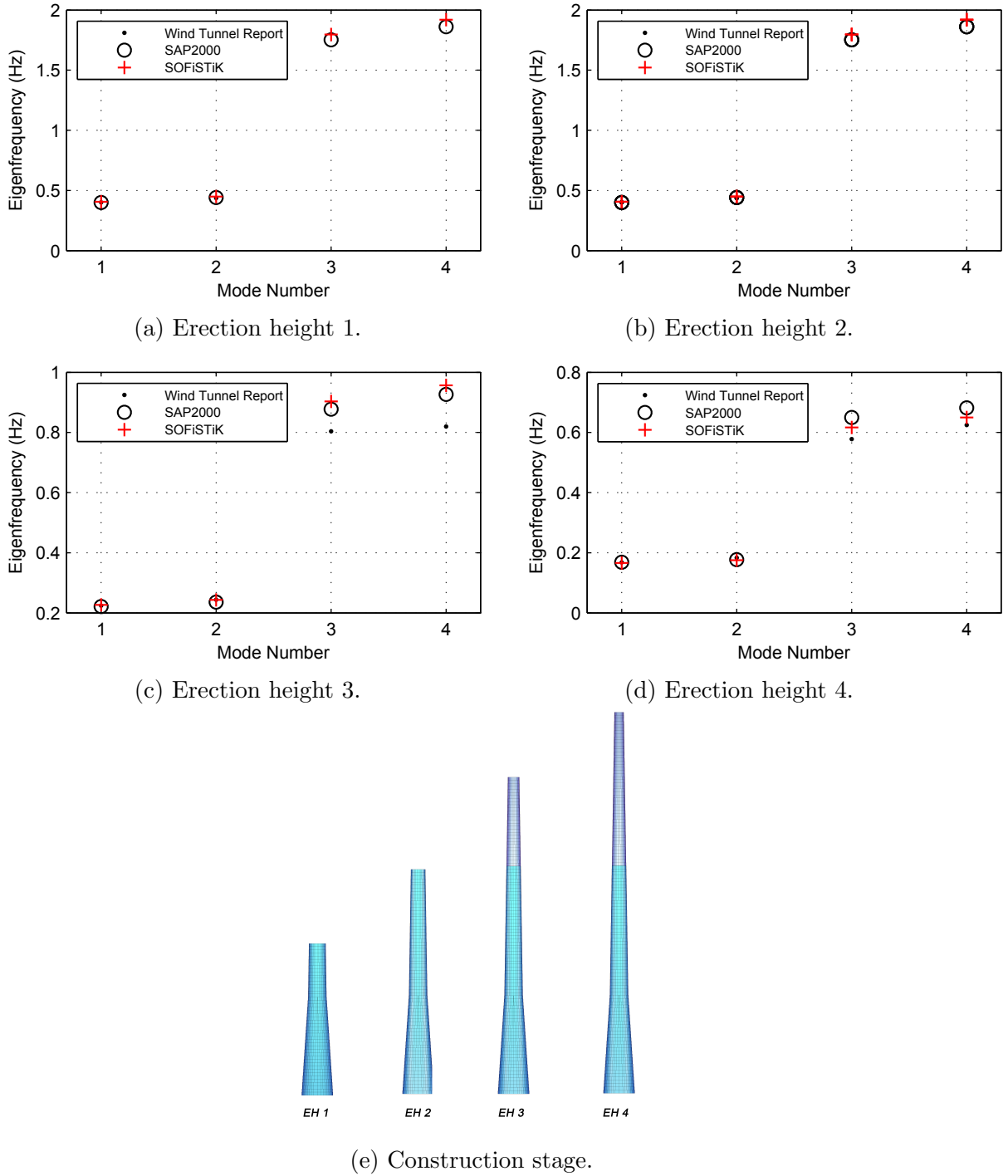


Figure 3.5: Comparison of eigenfrequency of tower in various erection stage.

numerical model, of which throughout the study is carried on. Based on the graphs and discussion of Figure 3.5, the numerical model in SOFiSTiK and SAP2000 are eligible for proceeding to the next step of simulation.

3.3.2 Wind-Structure Numerical Simulation

One of the methods used for Computational Fluid Dynamics simulation is Vortex Particle Method (VPM). VPM is based on grid free Lagrangian formulation of the Navier-Stokes equations, where the domain is discretized by particles carrying on vorticity. These particles are being convected due to free stream velocity as well as diffused. This representation yields the main advantages of low numerical diffusion, compact discretisation as the vorticity is strongly localized, implicitly accounting for the free space boundary conditions and a natural representations of the vortex creation process inherent in bluff bodies flow [5]. These concept is implemented inside a numerical software, VXflow [6].

VXflow is a numerical solver which works in two dimension fluid flow. To capture three dimensional response, one need to introduce a number of slices. Each slice represents particular cross section in a structure of a certain elevation. These representative slices then confronted by the wind, and the slices responses back hence deliver the result of displacements and forces for a number of time steps defined. Then the sectional fluid forces are multiplied with the height of each slices to obtain the applied total of its nodal load. The time step is dependent of the velocity of the wind and the number of panel (discretisation) introduced in the cross section definition. The relation defined in Equation 3.1 with dx the panel length, and \bar{U} is the wind velocity. This means the time step immediately change whenever one of these parameters changes.

$$\Delta t = \frac{dx}{\bar{U}} \quad (3.1)$$

VXflow works in two possible analysis: static and dynamic. The dynamic analysis enables user to compute dynamic response of the structure. This feature is used in order to capture aeroelastic and aerodynamic and problems, for instance the vortex induced vibration, buffeting, flutter, or galloping. This requires the supply of the modal data such as modal mass, frequency, modal damping (of critical), and mode shapes. The input of the modal data is obtained from finite element softwares. In this study, the modal data and mode shapes used are shown in Table 3.3 and Figure 3.6.

As previously explained, four erection heights were simulated in wind tunnel test. Only three of them are simulated in numerical solver VXflow, which are erection stages of elevation 174 m, 246 and 293 m. This is because the wind velocities of erection stage 119 m does not have significant response of vortex induced vibration. The simulation implements a constant wind velocity to model the smooth boundary layer of wind flow. The simulation of elevation 174 m and 246 m will not used further in the TMD simulation, only to show validation of the numerical model with wind tunnel test.

For freestanding tower study of erection 174 m, 246 m, and 293 m, four, five and six number of slices utilized for the simulation, respectively. These slices represent six

3.3. NUMERICAL SIMULATION

Table 3.3: Eigenfrequency and modal mass of tower Stonecutter bridge.

Mode	ω (1/s)	f (Hz)	T(s)	f-XX(%)	f-YY(%)	f-ZZ(%)
EH 2 (174 m)						
1	2.548	0.406	2.466	0	46.7	0
2	2.823	0.449	2.226	44.4	0	0
3	11.291	1.797	0.556	0	21.8	0
4	12.06	1.919	0.521	22.3	0	0
Total mass is 47207.67 ton						
EH 3 (174 m)						
1	1.429	0.227	4.397	0	39.9	0
2	1.528	0.243	4.111	37.6	0	0
3	5.671	0.903	1.108	0	22.1	0
4	6.014	0.957	1.045	22.1	0	0
Total mass is 54552.09 ton						
EH 4 (293 m)						
1	1.044	0.166	6.016	0	35.3	0
2	1.098	0.175	5.721	33.3	0	0
3	3.875	0.617	1.621	0	22.1	0
4	4.086	0.65	1.538	21.8	0	0
5	9.226	1.468	0.681	0	11.5	0
6	9.607	1.529	0.654	11.9	0	0
7	16.898	2.689	0.372	0	6.8	0
8	17.451	2.777	0.36	7.2	0	0
9	20.733	3.3	0.303	0	0	0
10	24.012	3.822	0.262	0	0	64.4
Total mass is 57924.013 ton						

representative section geometry of the tower in different elevation. The discretisation of panel length for the section is 0.5 m. Based on the wind tunnel report, the critical wind velocity for these erected stages are 27.5, 15–18, and 9.5 m/s, respectively. Angle of attack assigned for this simulation are 4°, 8°, and 0° respectively. The configuration of slices and geometry being inputted in VXflow could be seen in Figure 3.7.

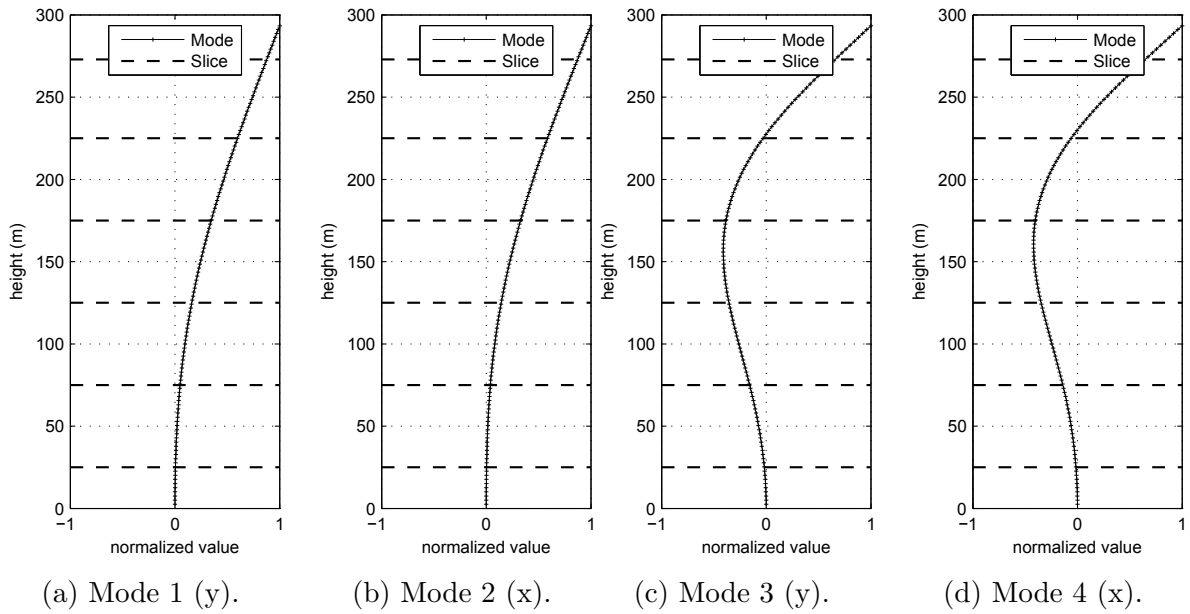


Figure 3.6: Mode shapes (SOFiSTiK) of fully erected tower.

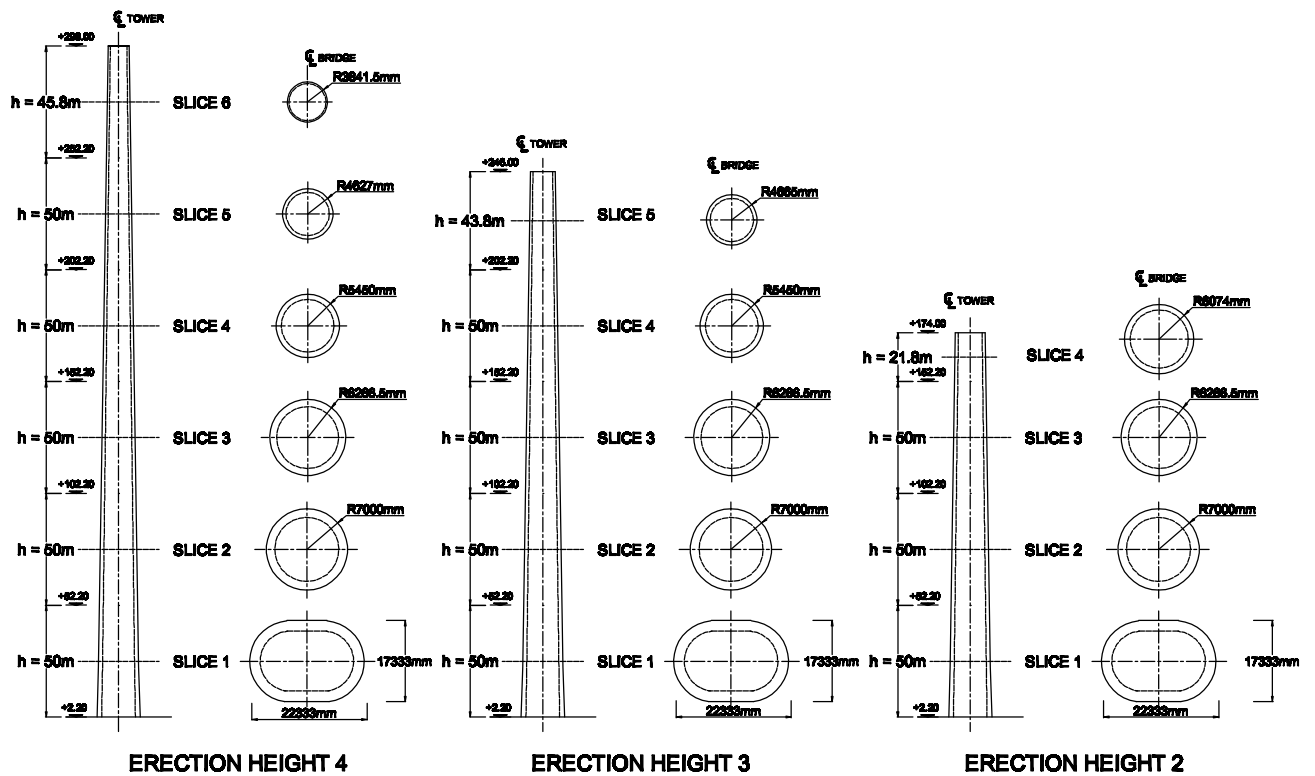


Figure 3.7: Tower input of slices and geometry for Vxflow.

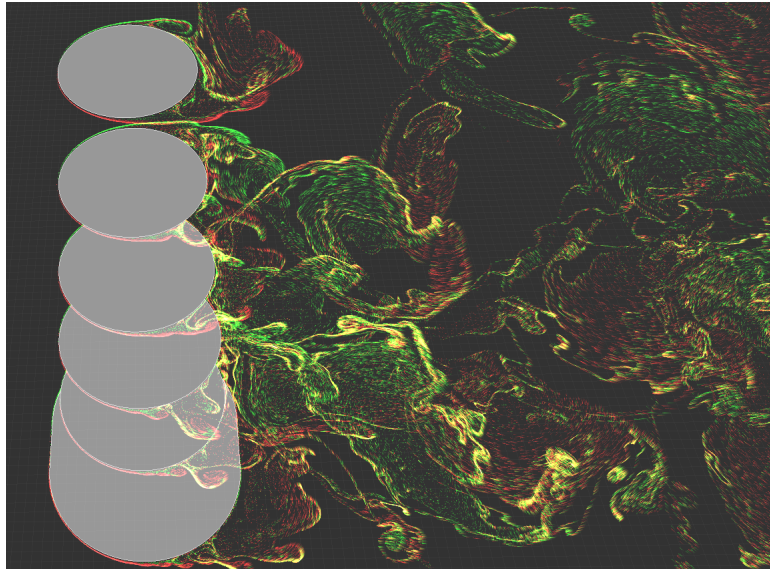
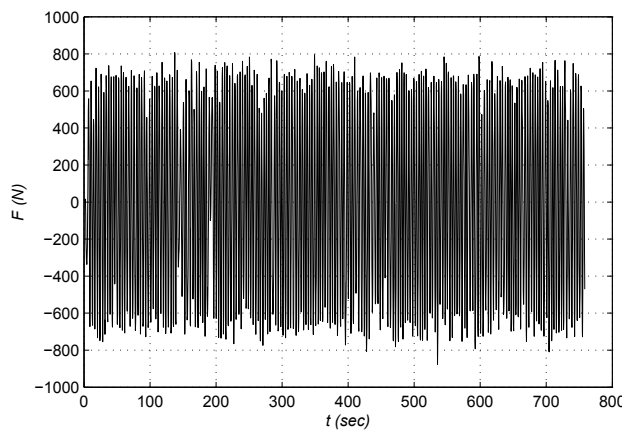
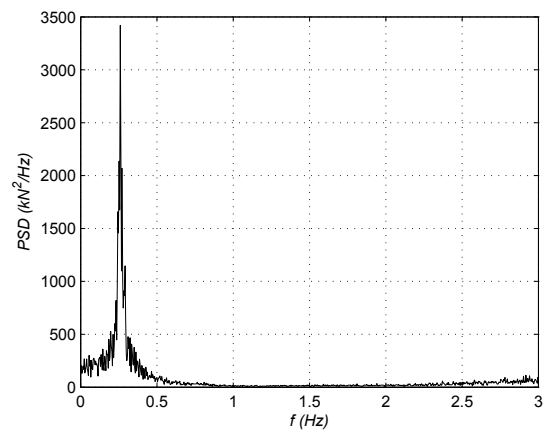


Figure 3.8: Multi slices dynamic pseudo 3D VXflow simulation.



(a) Forces signal from slice 6.



(b) PSD of forces signal from slice 6.

Figure 3.9: Forces signal which meet the first bending frequency in the direction of vortex induced vibration.

3.4 Result and Comparison with Wind Tunnel Test

One of the important parameters for computational fluid dynamics simulation is Reynolds number. Both the numerical solver and wind tunnel test has the same agreement of Reynolds number, which are within range 1 to 9×10^7 in full scale. After VXflow simulation, the displacement time histories from each slice obtained. These displacement are really important because they are representing the behaviour of vortex induced vibration. The tip displacement then refers to the displacement occur in the slice number six, which is the highest elevation of slices simulated in VXflow.

Full time series of tip displacement shown in Figure 3.10 which represents the value from simulation in erection height 2 (174 m), 3 (243 m), and 4 (293 m). The tip displacement time series shown in Figure 3.10 are processed further with Fast Fourier Transform to obtain the power spectral density spectrum. By this manner, it could be seen if the condition of the structure corresponds with lock-in phenomenon of vortex induced vibration.

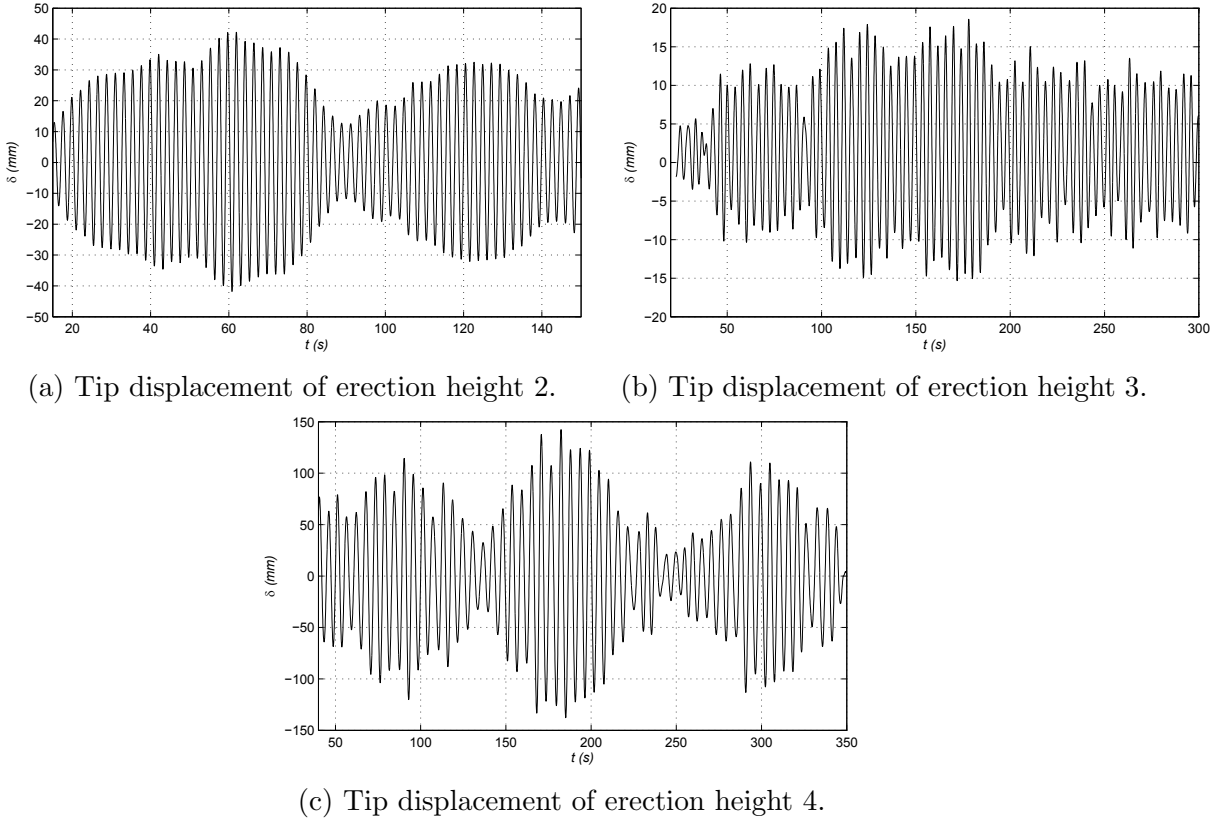


Figure 3.10: Result of displacement time series at the top of tower.

This is shown at Figure 3.11 that there are only one peak shows in each of psd plot which are in the frequency of 0.446 Hz, 0.250, and 0.182 Hz, respectively, which are near to the first bending mode of across wind direction for each erection stages (see Table 3.3, second mode). This brings to conclusion that the structure oscillates perpendicular

of wind direction caused by of vortex induced vibration.

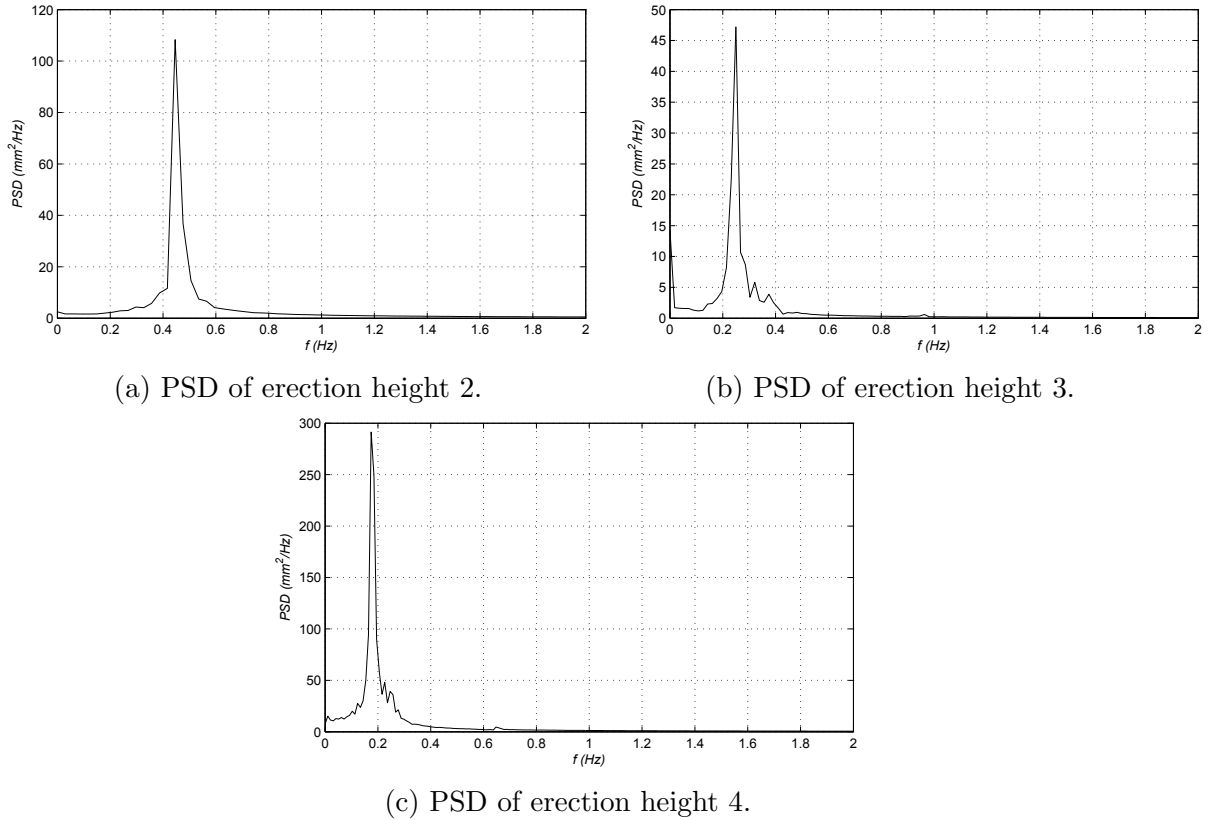


Figure 3.11: Power spectral density (PSD) of tip displacement in 3 different erection stages.

The maximum displacement obtained from the simulation are then compared with the result of wind tunnel test. The full comparison maximum tip displacement and other parameters are shown in Table 3.4. This simulation shows rather good result, with overall average discrepancy between numerical simulation and wind tunnel of maximum tip displacement around 21%.

Table 3.4: Comparison between Wind Tunnel (WT) and Numerical Simulation (NS).

Parameter	Erection 174 m		Erection 243 m		Erection 293 m	
	WT	NS	WT	NS	WT	NS
Max tip displ.	31 mm	42 mm	27 mm	19 mm	150 mm	156 mm
Strouhal num.	N/A	0.208	N/A	0.218	0.2	0.22
Wind speed	27.5 m/s	27.5 m/s	15 - 18 m/s	16.5 m/s	9.5 m/s	9.5 m/s
Wind angle	4°	4°	8°	8°	1°	0°

Chapter 4

Application of Tuned Mass Damper (TMD)

4.1 Design of TMD

From the Chapter 3 of the thesis, the maximum displacement response occurs on tip of the tower. This comes from the dominant mode shape, with already 60% of total modal mass accommodated in the first and second bending mode. This is shown comprehensively in Figure 3.6 and Table 3.3 of eigen vectors and eigen frequency with maximum value of modal displacement occurs in the top. Furthermore, the energy of the lateral vibration at the top of the tower are concentrated around 0.183 Hz as shown in Figure 3.11c. These peaks from power spectral density of displacement signal are close to the first bending mode of the Stonecutter Bridge. This characteristic leads to a determination of a proper location of tuned mass damper, which should be deposited near the top of tower.

The tuned mass damper (TMD) in Stonecutter Bridge tower is installed inside the hollow section, in a form of a mass attached to surrounding walls with means of spring and damper and an addition of rope to enable the mass to swing. The TMD's center of mass intersects with the center of the tower, thus creating a symmetric geometry system. As previously said, the TMDs' locations are in position to reduce the tip displacement. Hence the single TMD is deposited at the top of the tower.

In the section 2.5, it is mentioned about Den Hartog's optimum parameter of designing tuned mass damper. Those parameters are frequency ratio κ and damping ratio ζ_d . These two parameter will be carried out inside all the simulation of TMD modeling. In addition, there is one more important parameter which is mass ratio of TMD (μ). The mass ratio refers to the ratio between total mass of TMDs and the equivalent mass of

the controlled mode, which define as

$$\mu = \sum_{i=1}^N \frac{m_i}{M}, \quad (4.1)$$

where m_i is the mass of TMD, N represents the number of TMDs, and M is the equivalent mass of the controlled mode. In case of single TMD, the mass ratio directly associated to the mass of single TMD.

4.2 Finite Element Modeling of the TMD

Tuned mass damper in finite element software is modeled as a combination of a mass and a spring element (or link element). The TMD acts like a pendulum with its own stiffness k_d , damping c_d and natural circular frequency ω_d . The TMD then attached with the main system in a certain position. During the excitation, the TMD moves along with the main system and its movement dissipates the energy received by the main system.

To make a verification in finite element software of a TMD model, a single degree of freedom structure consists of a lumped mass m_m , a stiffness k_m , and damping c_m is modeled. One TMD attached to the lumped mass m_m and it is possible to move in horizontal direction. A series of harmonic excitation with circular frequency of ω is applied on the mass and the dynamic amplification response due to these excitation then collected. The configuration of this verification model is shown in Figure 4.1.

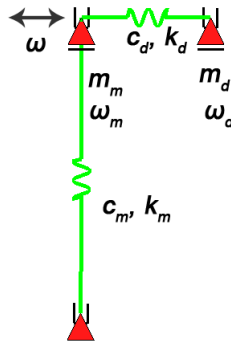


Figure 4.1: Model consists of a sdf with a TMD system in SOFiSTiK.

The properties of sdf system used for the simulation are stated below

$$m_m = 15 \text{ ton} \quad k_m = 450 \text{ kN/m} \quad c_m = 10.602 \text{ kN s/m} \quad \zeta_m = 0.05 \quad (4.2)$$

with the equation 2.33 one can get the $\kappa_{opt}(= 0.990)$ to design the property of TMD

4.2. FINITE ELEMENT MODELING OF THE TMD

taking $\mu = 0.01$

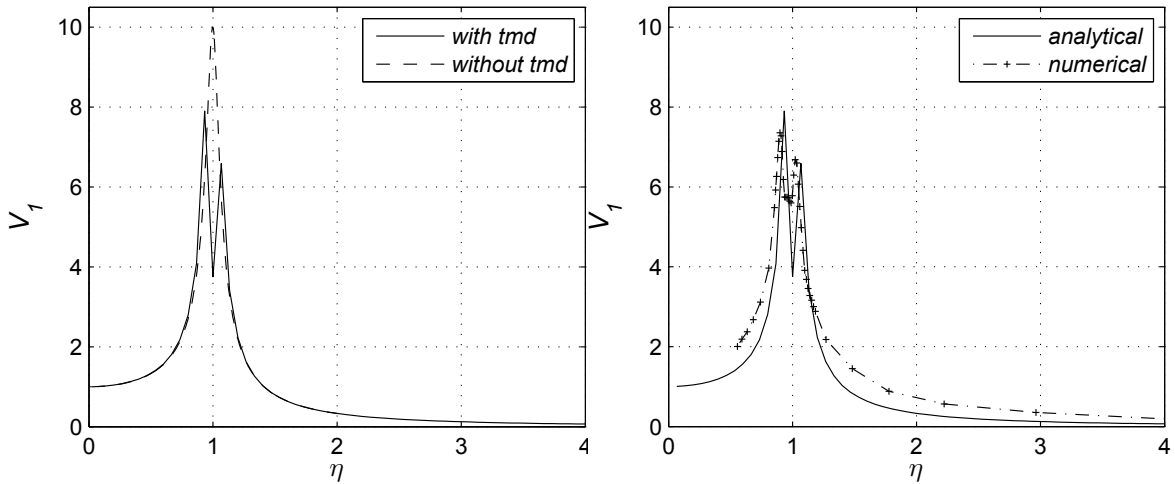
$$m_d = 0.15 \text{ ton} \quad k_d = 7.35 \text{ kN/m} \quad c_d = 0.04 \text{ kN s/m} \quad \zeta_d = 0.02 \quad (4.3)$$

Harmonic excitation forces which applied in the system are defined as below:

$$F = (1 \text{ kN}) \sin \omega t = (1 \text{ kN}) \sin \frac{2\pi}{T} t \quad (4.4)$$

with periods of excitation T are varied from 0.2 sec to 1.6 sec to obtain different value of ratios of excitation η (compared with equation 2.32).

Manual calculation of equation 2.31 had been done to observe the tendency responses of the whole system being loaded in different values of excitation. Taking $\alpha = 0.5$, one can plot the result of calculation in Figure 4.2. In the similar way, the numerical simulation with a series of period excitation had been executed. The plot shows how the changes of dynamic force amplification with respect to static force in different values of excitation.



(a) With and without TMD.

(b) Analytical and numerical.

Figure 4.2: Comparison of dynamic amplification function in two-dof system.

In Figure 4.2 the different values of excitation represent by η , which is the ratio between excitation frequency and frequency of the sdof system. In the point of resonance which happens in $\eta = 1$, the value of V_1 in Figure 4.2a shows the peak. But then when a TMD is added the peak splitted into two with lower magnitude of V_1 . This reduced peak due to added TMD also shown in numerical simulation, with similar tendency of manual calculation. The comparison between manual calculation and numerical simulation is shown in Figure 4.2b. The result of comparison in Figure 4.2b, the manual and numerical calculation shows 10% discrepancy. Looking at this result, one can proceed to the next step of TMD simulation.

The TMD is then applied inside the tower of Stonecutter bridge. The TMD consists of a sphere mass, possibly made of concrete, and attached to the perimeter wall with means of damping and spring element. Another attribute to be added is the rope to enable the mass to swing. The physical illustration of TMD inside the reference object is shown in Figure 4.3.

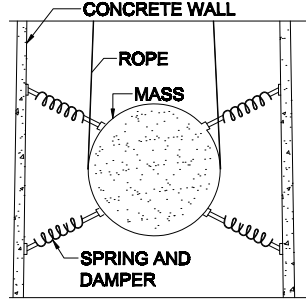


Figure 4.3: Tuned mass damper inside tower.

4.3 Numerical Simulation of TMD with VXflow

To take into account the property and effect of tuned mass damper inside VXflow, one has to calculate the effective damping of a structure with TMD altogether. The effective damping is calculated through a free vibration simulation of the tower attached with the tuned mass damper. The tuned mass damper represented by an extra spring, mass, and damping on the top the finite element model of the tower and the properties of which determined by equation 2.33 and 2.34. Taking the ratio of mass, $\mu = 0.005$, and mass of predominant frequency, which is mass of first bending mode in the direction of vortex induced vibration, 19288 ton, leads to the following properties of TMD:

$$m_d = 96.44 \text{ ton}, \quad (4.5)$$

$$\kappa = \frac{1}{1 + \mu} = \frac{1}{1 + 0.005} = 0.995, \quad (4.6)$$

$$\zeta_d = \frac{3\mu}{8(1 + \mu)^3} = \frac{3(0.005)}{8(1 + 0.005)^3} = 0.043, \quad (4.7)$$

$$k = 4\pi^2 m f_d^2 = 4\pi^2 (96.44) (0.995 \times 0.175)^2 = 115.44 \text{ ton/s}^2, \quad (4.8)$$

$$c = 2\zeta_d \sqrt{km} = 2(0.043) \sqrt{(115.44)(96.44)} = 9.07 \text{ kN s/m}. \quad (4.9)$$

Following the similar approach of section 4.2, the finite element model of tower and TMD are constructed. Using the previous obtained model described in section 3.3.1, the tuned mass damper attached in the top of the tower as shown in Figure 4.4.

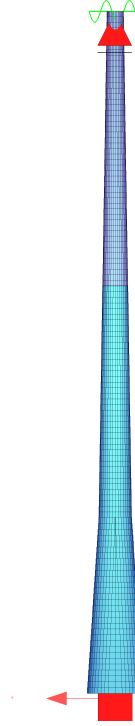


Figure 4.4: Tower with tuned mass damper model in SOFiSTiK.

Effective Damping Calculation

The free vibration simulation of the structure represented by applying an impulse force of 10000 kN in the top of the tower with time step of 0.1 s for 120 seconds. Afterwards the tower deflects and as the time developed, the tower and TMD starts to interact with each other thus create a damped oscillation. The displacement response of the tower along the time are recorded and observed. In the finite element software SOFiSTiK, the numerical approximation procedure for time history analysis is done in the module of *ASE*, while the load function of time history analysis is defined in module *Sofload*.

Displacement time history of a node in the tower is taken and shown in Figure 4.5. From this figure, the calculation of effective damping is according to the equation 2.14 and elaborated below:

$$\Lambda = \frac{1}{n} \ln \frac{x(t_1)}{x(t_1 + nT)} = \frac{1}{1} \ln \left(\frac{126.748}{44.88} \right) = 1.038, \quad (4.10)$$

$$\zeta = \frac{\Lambda}{\sqrt{4\pi^2 + \Lambda^2}} = \frac{1.038}{\sqrt{4\pi^2 + 1.038^2}} = 0.163. \quad (4.11)$$

The value of effective damping $\zeta = 0.163$ is used for the simulation of VXflow to obtain the coupled response between wind, tower and tuned mass damper. This effective damping replaces the previous modal damping inputted in VXflow in the terms of modal data of the tower.

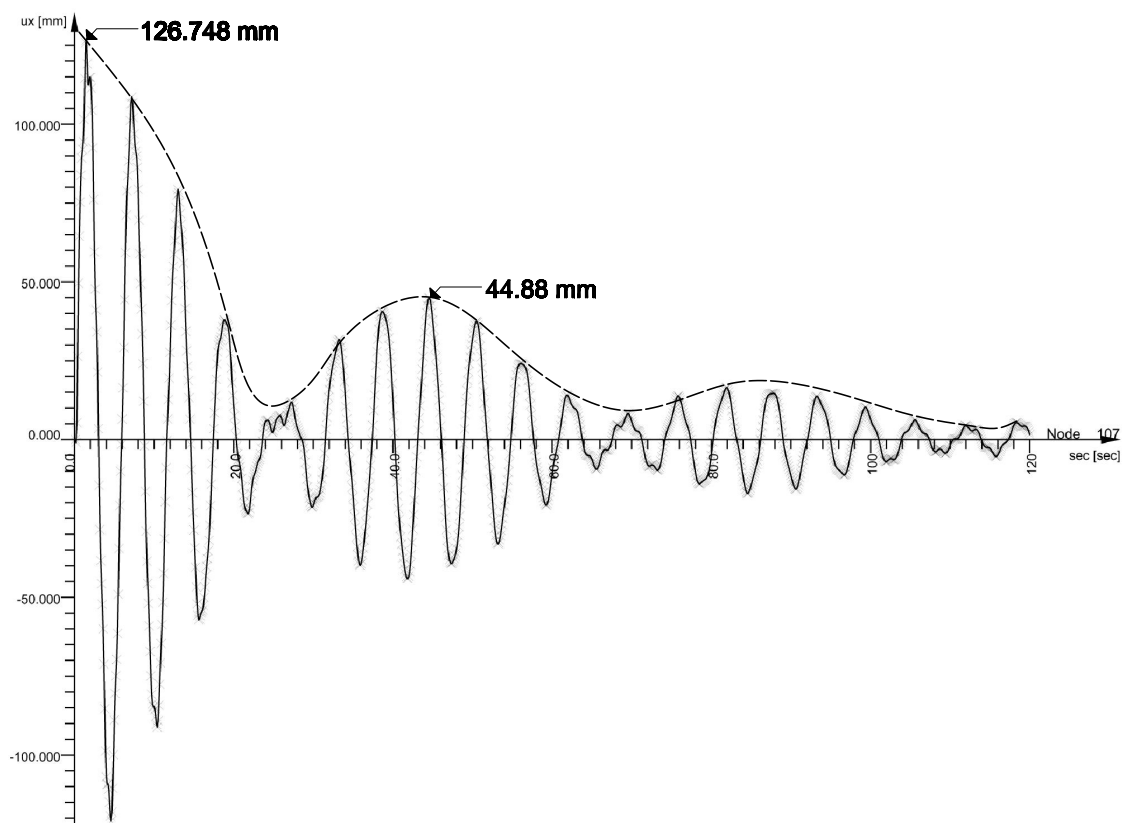


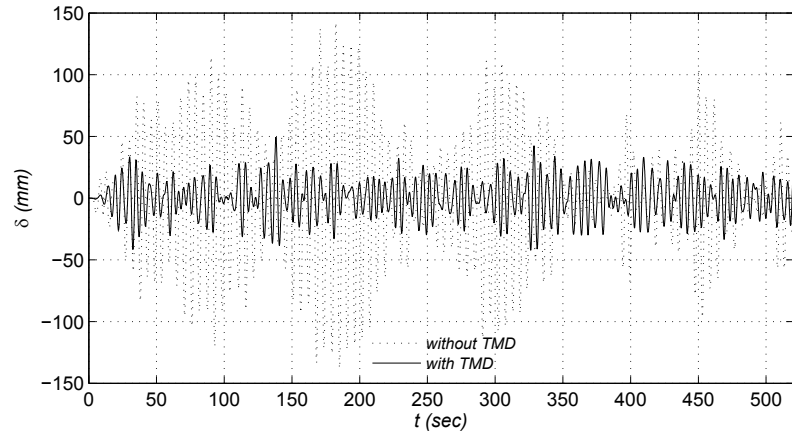
Figure 4.5: Decaying displacement response time histories of the tower with single TMD.

Simulation and Result

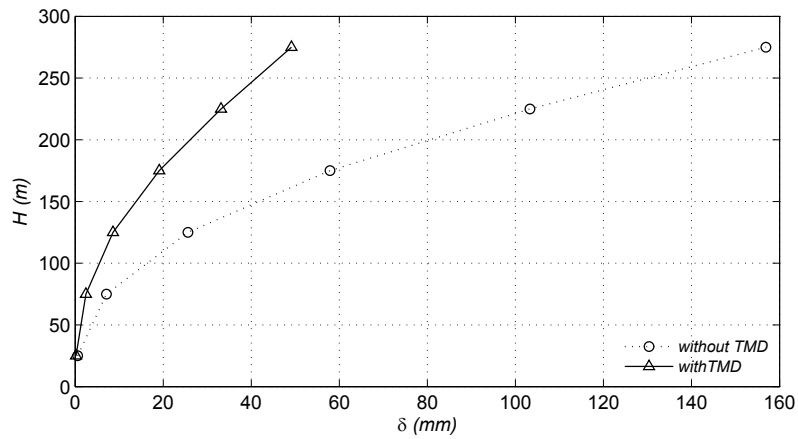
The displacements of the structure after applying the TMD are reduced. The maximum displacement reduction along the height averagely reach 66.86%. The reduction happened in every slice of the structure. The table and graph showing the maximum displacement reduction shown by Table 4.1 and Figure 4.6.

Table 4.1: Reduction of maximum displacement (mm) in different elevation.

Type	H = 25m	H = 75m	H = 125m	H = 175m	H = 225m	H = 275m
Without TMD	0.55	7.11	25.62	57.89	103.31	156.91
With TMD	0.19	2.43	8.60	19.12	33.13	49.13
Reduction	65.24%	65.89%	66.41%	66.98%	67.93%	68.69%



(a) Time history displacement at top of the tower.



(b) Maximum displacement.

Figure 4.6: Comparison of displacement time histories.

4.4 Numerical Simulation of TMD with FE Software

The aeroelastic loads calculated by the simulation in the VXflow environment is obtained and employed as nodal forces acting on the tower's finite element model. The forces collected used as inputs for structural analysis in SOFiSTiK. In this sense, the analysis becomes uncoupled. It is because the aeroelastic interaction between wind and structure due to this aeroelastic phenomena is no longer captured in finite element software. On the other hand, the the detailed responses such as internal forces and accelerations in the structure could be observed in more straightforward manner. The other advantage is TMD properties and behavior could be observed in more detailed study.

Haselbach, et al [25] analyzed the comparison of fully coupled and uncoupled simulation of an offshore wind turbine structures. The fully coupled aero-hydro-elastic simulation is done in HAWC2 and uncoupled load predictions in the finite element software Abaqus. The background behind the uncoupled analysis due to frequently separate analysis and

manufacturers of substructure and tower. At the end Haselbach shows the displacement and mean load responses reasonably match but is still present a discrepancy of 25% amplitude of forces and moment in substructure joint.

4.4.1 Wind-Structure Simulation

After a wind simulation has finished, VXflow provided the time histories forces of each slice. These forces extracted from VXflow are applied on a point of elevation corresponds to the slice's elevation inside tower numerical model. In this way, a time history analysis then performed to obtain real time displacement and real time internal forces. The responses to this dynamic loading is calculated using numerical approximation procedures. In SOFiSTiK the alpha method or Hilber-Hughes-Taylor, which is also an extension of Newmark method, is implemented. With the Hilber-Hughes-Taylor method it is possible to introduce numerical dissipation without degrading the order of accuracy [12].

Another parameter necessary for numerical analysis is damping value. SOFiSTiK could not carry out direct (Lehr's) damping in time history calculation, so that Rayleigh Damping have to be utilized. Rayleigh damping makes use the proportionality of the damping matrix to either stiffness or the mass matrix. The modal damping ratio has defined previously by Equation 2.13 with ζ_k is modal damping ratio, α and β are the factors of stiffness and mass proportional damping respectively and ω_k is natural circular frequency.

In SOFiSTiK, these two factors α and β are calculated using input of two expected damping, ζ_1 and ζ_2 in between two natural circular frequency, ω_1 and ω_2 and expressed in Equation 4.12 and 4.13. However for the sake of accuracy, the effective damping is again checked through a free vibration analysis.

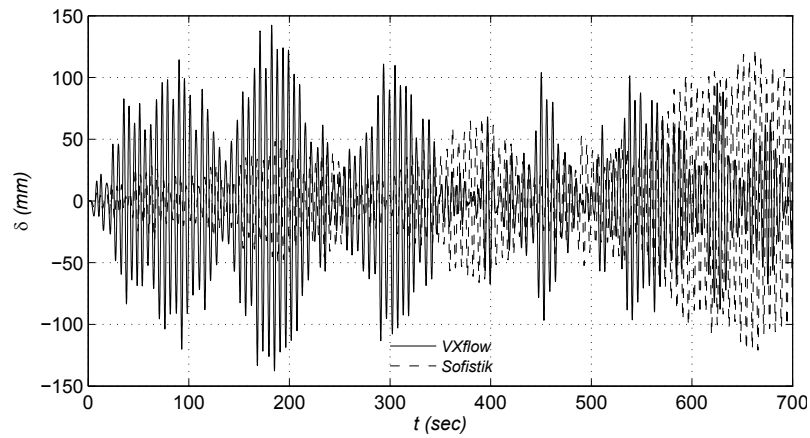
$$\alpha = 2 * \frac{\zeta_2 \omega_2 - \zeta_1 \omega_1}{\omega_2^2 - \omega_1^2} \quad (4.12)$$

$$\beta = 2 * \omega_1 \omega_2 \frac{\zeta_1 \omega_2 - \zeta_2 \omega_1}{\omega_2^2 - \omega_1^2} \quad (4.13)$$

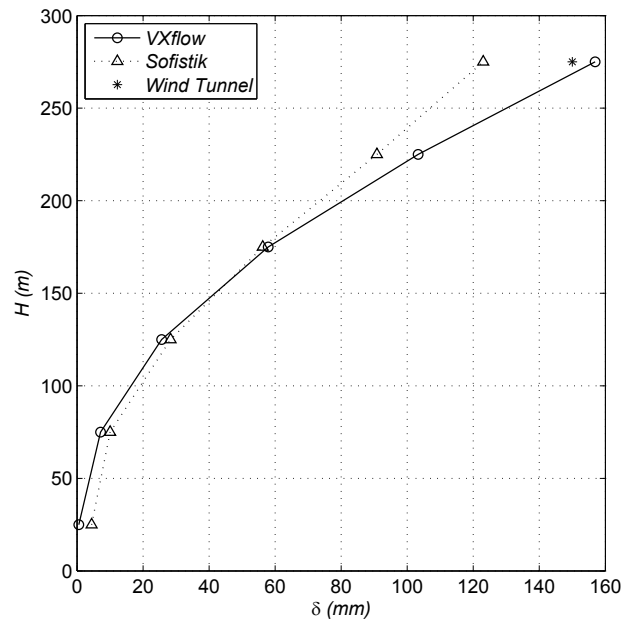
The result obtained from this simulation are then compared with the result of coupled analysis done in VXflow environment. The time histories of top displacement is showed in Figure 4.7a and the maximum displacement of selected section according to the elevation of slices shown in Figure 4.7b.

These two figures shows discrepancy of maximum displacement between VXflow and Sofistik approach with average value of 20%. Displacement on the bottom tower in Sofistik simulation shows smaller magnitude than in VXflow simulation, but then on the

top regions, the VXflow gives bigger magnitude. Looking at this result, one can proceed to observe and analyze deeper by putting TMD in this uncoupled wind simulation of finite element software of SOFiSTiK.



(a) Time history displacement at top of the tower.



(b) Maximum displacement.

Figure 4.7: Comparison of displacement time histories between VXflow, Sofistik, and Wind Tunnel.

Wind-Structure-TMD Simulation

The aeroelastic loads which obtained from preceding wind structure simulation of VXflow then applied inside a complete finite element model of a tower with TMD in SOFiSTiK. The finite element model described in section 4.3 is used again with input of time histories of nodal load acquired from CFD solver VXflow. This simulation is done to obtain agreement of the response of structure with TMD between the coupled analysis of VXflow and uncoupled analysis of Sofistik. The agreements of these responses is required so that the later parametric simulations are valid to be executed and analyzed.

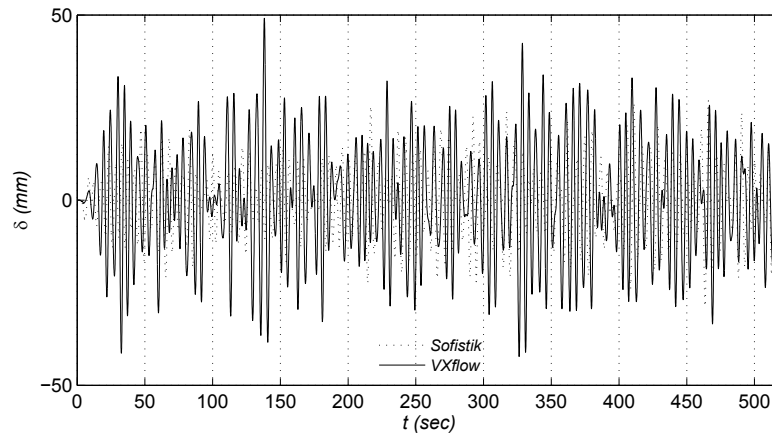
Different from the VXflow approach which only take out the effective damping, SOFiSTiK can model the real property of TMD and thus detailed analysis regarding the behavior of structure due to wind simulation could be performed.

The maximum absolute displacement observed from both of approach shown in Figure 4.8b. It can be seen that the result of maximum displacements between the uncoupled and coupled model are pretty reasonable in the bottom half of the tower, but not in the top half of the tower. However, since the simulation model of both methods without TMD has already 25% difference, it is expected that the simulation using TMD will also have discrepancies. Another way to look at this comparison is by comparing the reduction rates of maximum displacement due to added TMD.

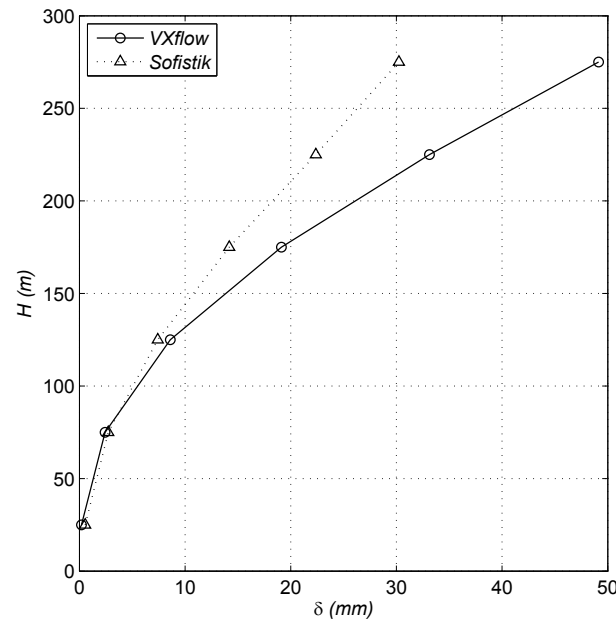
Figure 4.8c shows the reduction rate of displacement due to added TMD. Sofistik gives overall gives higher reduction rate than VXflow, with average 76.62%. Meanwhile, average of reduction rate in Sofistik simulation is 66.86%. The reduction rate between the two methods show only 15% difference. It is reasonable to say that the approach using uncoupled model is afterall not too bad.

4.4.2 Parametric Simulation TMD

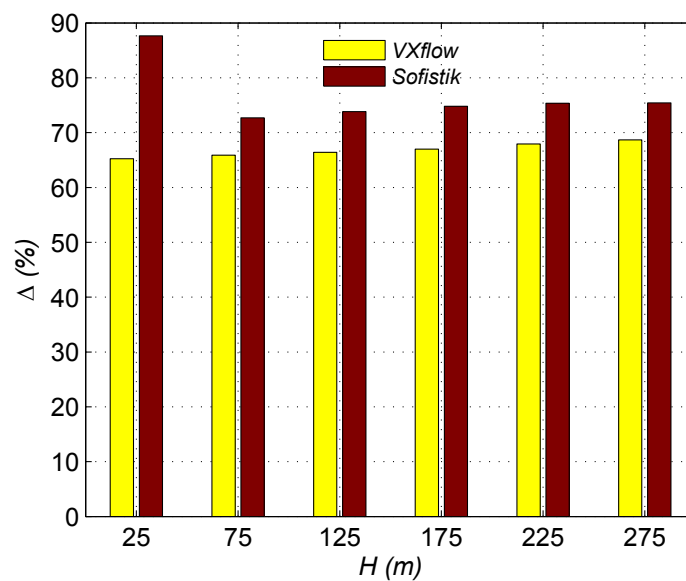
According to Moon [18], tuned mass damper will give more benefit if installed as multiple distributed tuned mass dampers along the height instead of one single TMD at top of structure. The benefits are regarding the space, installation, construction, and reliability. However, Moon concluded that single TMD performs slightly better than multiple TMD with difference of 5% reduction rate. By distributing TMDs vertically with multiple small TMDs at each level, their installation become easier, and the space remaining becomes bigger. It is also proved that with multiple TMD, not only first mode can be effectively controlled. Lastly, there is no substantial loss of effectiveness for motion control of slender structure. Another publication by Elias and Matsagar [20] shows when the position of the multiple tuned mass damper takes into account the location of maximum modal displacement of predominant frequency, the response of the system is improved. This system is even better than putting all multiple TMDs at the structure's top.



(a) Time history displacement at top of the tower.



(b) Maximum displacement.



(c) Displacement reduction rate.

Figure 4.8: Comparison of displacement responses of tower with TMD model.

Based in these presumptions, there is a need to observe the behavior of multiple TMD and a single TMD attached in the reference structure. In this case, the comparison of both structure is made based on the properties shown in Table 4.2 while the illustration of finite element model shown in Figure 4.10.

Table 4.2: Property of TMD.

No. TMD	μ	ζ_d	κ	m_d (ton)	k_d (kN/m)	c (kN s/m)
1	0.5%	0.043	0.995	96.44	115.44	9.07
5	0.5%	0.043	0.995	19.288	23.09	1.82

The result shows that both damper configurations are effective to reduce the vibration due to vortex induced vibration. Single TMD reduces 75% and 68% of the peak displacement and peak acceleration, respectively, while multiple TMD reduce 69% and 67% of the peak displacement and rms acceleration, respectively. The table showing complete result is in Table 4.3. The figures shown in Figure 4.9.

This finding leads back to Moon’s and Elias & Matsagar’s conclusion that with respect to degree of simplicity in construction and installation of TMD as well as the limitation of space inside the tower, it is necessary to use multiple TMD instead of single TMD. In addition, the result also shows that there are no substantial loss of reduction capacity regarding installation of multiple TMD compared to single TMD.

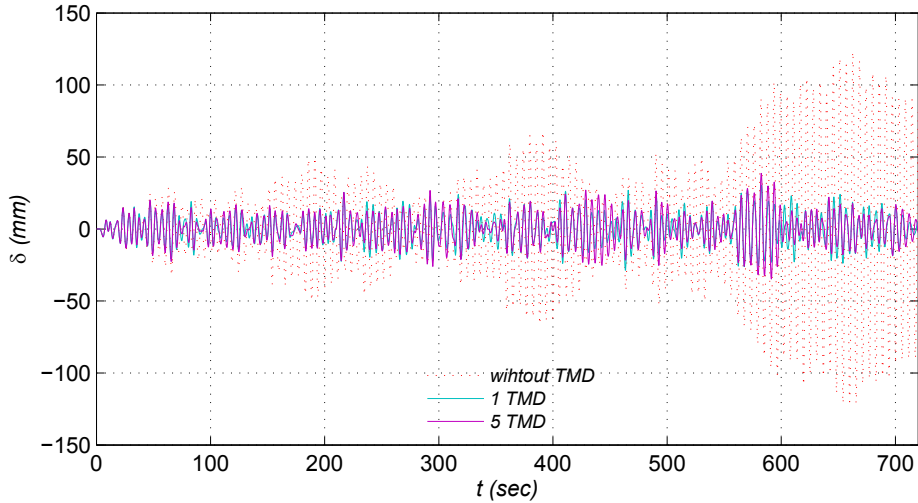
Table 4.3: Comparison of tower respons: without, with 1 TMD, with 5 TMD.

Case	Peak disp.	Peak acce.
No damper	123.0277 mm	156.33 mm/s ²
One damper	30.24 mm	49.85 mm/s ²
Five damper	38.63 mm	51.74 mm/s ²

Distribution TMD

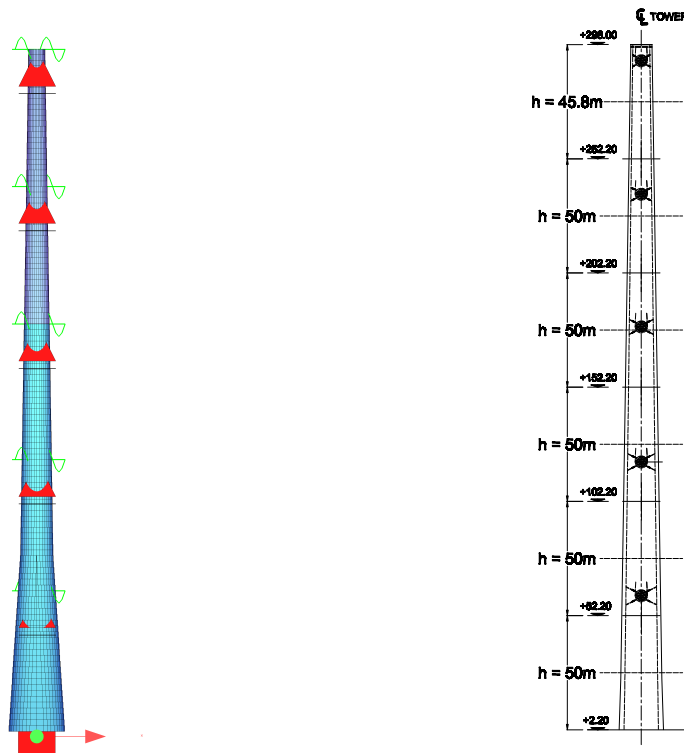
Some publications regarding the multiple TMD concern about the vertical distribution along the height of the reference structure. Moon [18] deposited four TMDs starting from mid-height of a structure until its top. On the other hand Yang, et al [21] distributed multiple small TMD only at the top of a structure. Another study of Elias and Matsagar [20] showed that the TMD that installed in the maximum modal displacement of predominant frequencies of the structure benefited the responses. However, neither of these publications attempted to compare the optimum effects in case of different TMD distribution along the height of the structure.

Therefore, four types of distribution system are here simulated. Five numbers of TMD distributed in four different schemes. The first scheme is to try to put all five TMDs



(a) Displacement time history.

Figure 4.9: Comparison of responses between structure: without TMD, with 1 TMD, with 5 TMD.



(a) Multiple TMD.

(b) Physical illustration.

Figure 4.10: Multiple tuned mass damper model illustration.

clustered in the top of the tower. The clustered model separate each TMD one from another with only five meter gap. The second scheme is to put the TMDs equally spaced until the middle of the tower. The third scheme is to put the TMDs following a polynomial function, namely second order polynomial. The last one is then to try not

only distribute based on spacing but also based on mass. Hence, the last simulation is distribute the TMDs in both mass and spacing following the polynomial second order function. For all first three schemes, the property of tuned mass dampers are $m_d = 19.29$ ton, $k_d = 23.09$ kN/m, and $c_d = 1.82$ kN s/m. The fourth scheme will only differ in terms of mass, but the spacing will be same with the third scheme. The coordinates of the dampers for each scheme are shown in Table 4.4.

Table 4.4: Coordinates of different schemes of multiple TMD distribution.

TMD no.	Clustered	Equal	Polynom (Spacing)	Polynom (Mass)
1	274.35 m	145.59 m	145.59 m	1.75 ton
2	279.07 m	183.09 m	225.59 m	7.01 ton
3	286.15 m	220.59 m	270.59 m	15.78 ton
4	290.87 m	258.09 m	290.59 m	28.06 ton
5	295.59 m	295.59 m	295.59 m	43.84 ton

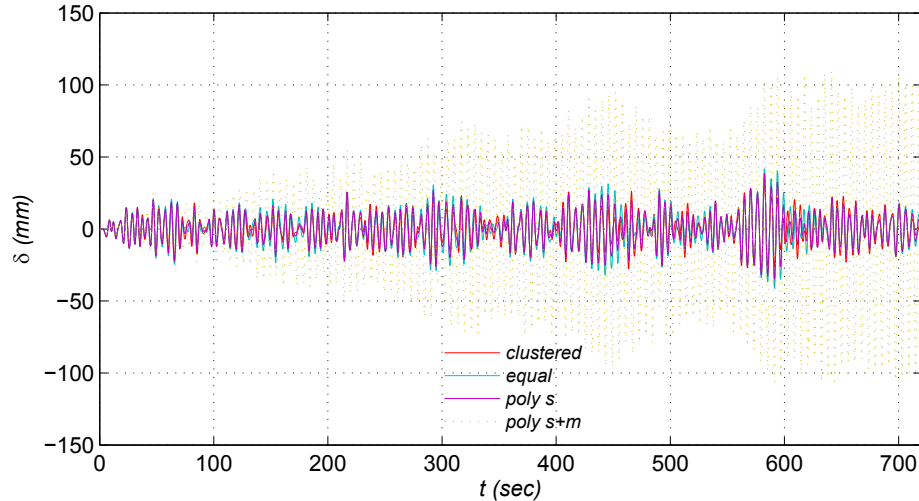
Deflection of the tower is one crucial point since the definition of damage in a structure commonly measured based on it. Motion perception which influence the human discomfort is normally described in the term of acceleration. These are the reason, why responses to be observed in this study are displacement and acceleration at the top of the tower.

The first comparison is the distribution of TMD. There are five different simulations conducted in this study, which are: clustered of TMD in the top of structure, equal spacing of TMD from mid-height until the top, spacing which follows polynomial function with equal mass distribution from mid height to top, and and mass and spacing which follow polynomial function from mid-height to top.

Table 4.5: Comparison of tower respons: Distribution of TMD.

Case	Peak disp.	Reduction Rate	Peak acce.	Reduction Rate
Clustered	33.053 mm	73.13%	50.08 mm/s ²	68%
Equal	41.76 mm	66%	55.65 mm/s ²	64.4%
Poly s	38.63 mm	68%	51.74 mm/s ²	67%
Poly m+s	109.56 mm	10.9%	135.58 mm/s ²	13.3%

From the comparison of Table 4.5, the clustered distribution performed the best to reduce responses in terms of peak displacement and peak acceleration. This makes sense since the clustered distribution shares similarity to the case of single TMD. On the other hand, polynomial distribution performed better response compared to equal distribution. Based on modal displacement curve of first bending frequency of the structure (see Figure3.6b), the shape follows the curve of polynomial function. The



(a) Time history of tip displacement.

Figure 4.11: Comparison of tip response with distribution case.

influence of this mode shape curve benefited the polynomial distribution compared to equal spacing. When both spacing and mass distributed following polynomial distribution, the responses not shows any significant displacement reduction.

Mass Ratio

Mass ratio is an important matter in multiple tuned mass damper system. Finding a right ratio will be a key to have an optimum expected response with reasonable construction cost. When the mass is too big, it will require bigger cost and more complicated method of installation. When the mass is too small, then the response expected from the system will not be satisfactory.

The controlled mode used for analyzing the structure is first bending mode in the direction of vortex induced vibration. This is based on the fact that first bending mode vibrates in the same direction corresponds to vortex induced vibration with highest ratio of participated mass. This arguments also supported by the spectra of displacement and spectra of forces in Figure 3.11 and 3.9. It means the reference equivalent mass to be used for the mass ratio calculation is taken as the participated mass of mode two which is 19288 ton. Eight number of mass ratio are simulated to see the trend of response. For this case, a fixed amount of TMD is set as 5 for lateral direction. A constant frequency ratio κ is taken as 0.990, and the damping ratio of TMD ζ_d is set as 0.043. List of properties used in this variation of mass ratio given in Table 4.6.

There are two components to be observed to determine the best performance of mass ratio of TMD: displacement and acceleration. Both of these responses are observed in the top of the tower. Mass ratio of 1.5% gives smallest magnitude of displacement

Table 4.6: List of Mass Ratio Properties used in Simulation.

No.	μ	m_d (ton)	k_d (kN/m)	c (kN s/m)
1	0.25%	9.64	11.54	0.91
2	0.50%	19.29	23.09	1.81
3	0.75%	28.93	34.63	2.72
4	1.00%	38.58	46.17	3.63
5	1.25%	48.22	57.72	4.54
6	1.50%	57.86	69.26	5.44
7	1.75%	67.51	80.80	6.35
8	2.00%	77.15	92.35	7.26

Table 4.7: Maximum displacement in variation of mass ratio.

Parameter	Mass Ratio							
	0.25%	0.50%	0.75%	1.00%	1.25%	1.50%	1.75%	2.00%
Displ. (mm)	70.31	55.68	51.57	50.34	50.21	50.42	51.36	53.21
Accel. (mm/sec ²)	52.65	41.77	38.40	34.30	29.76	27.79	28.29	28.88

with 82.2% reduction rate. On the other hand mass ratio of 1.25% gives the smallest magnitude of acceleration with 59.2% reduction rate. This means either mass ratio 1.25% or 1.5% could be chosen for the optimum performance of TMD. However, in terms of construction cost, smaller mass ratio will benefited the investors economically. According to this condition, mass ratio 1.25% is selected as the optimum TMD properties. Final optimum properties of TMD is then (for single TMD):

$$m_d = 241.10 \text{ ton} \quad (4.14)$$

$$\kappa = \frac{1}{1 + \mu} = \frac{1}{1 + 0.0125} = 0.988 \quad (4.15)$$

$$\zeta_d = \frac{3\mu}{8(1 + \mu)^3} = \frac{3(0.0125)}{8(1 + 0.0125)^3} = 0.067 \quad (4.16)$$

$$k = 4\pi^2 m f_d^2 = 4\pi^2 (241.10)(0.988 \times 0.175)^2 = 284.34 \text{ ton/s}^2 \quad (4.17)$$

$$c = 2\zeta_d \sqrt{km} = 2(0.067) \sqrt{(284.34)(241.10)} = 35.19 \text{ kN s/m} \quad (4.18)$$

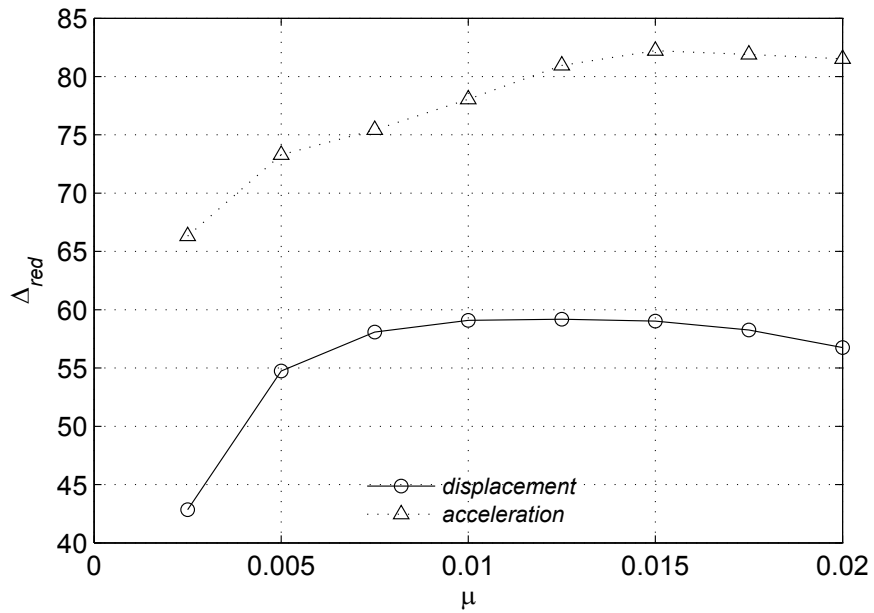


Figure 4.12: Reduction ratio of maximum tip displacement and acceleration.

Chapter 5

Conclusion

5.1 Summary

This thesis studies the aeroelastic phenomena which is the discipline concerned of significant interaction between aerodynamic forces and structural motions and creates self excited forces. One of the self excited forces that often creates problem in slender vertical structure is called vortex induced vibration. Shedding of vortices in the wake region produces across wind direction forces and in certain limit can fail the structure. Strouhal number plays an important role influencing this phenomenon, as engineer should avoid the natural frequency meets shedding frequency of the vortices in the wake region.

The reference structure used in this thesis is the bridge tower of Stonecutter bridge which have circular cross section. For aeroelastic analysis, Reynolds number plays important role to observe the separation point of circular section which affects the shedding of vortices. The Reynolds number of the reference object is in the scale of 10^7 , which is in the transcritical region with turbulent separation based on Schewe [10]. Two methods to measure the vortex induced vibration phenomena are experimental method using wind tunnel test and numerical method using computational fluid dynamics software. Wind tunnel test is conducted by BMT Fluid Mechanics [4] and the computational fluid dynamics is done inside VXflow solver developed by Morgenthal [6].

The comparison between numerical and experimental method for predicting the vortex induced vibration phenomena is done in three different erection stages of reference structure. Having validated the result, the tuned mass damper as the response control is added into the reference structure to reduce the unfavorable responses. There are two methods used for predictiong the response, coupled analysis and uncoupled analysis. The coupled anaysis done inside VXflow simulation by adding the effective damping of the structure and TMD altogether. The effective damping is obtained from free

vibration analysis in finite element software. The uncoupled method make use of the aeroelastic loads acquired from VXflow solver and applied in the corresponding position in finite element model of SOFiSTiK. The uncoupled model is done in order to observe the comprehensive responses of the tower itself, detailed properties of TMD, as well as the effects of multiple TMD to enhance altogether structural responses. The uncoupled procedure is also done by Haselbach [25].

5.2 Conclusion

Finite element model of Stonecutter bridge tower shows accurate natural eigen frequencies with respect to wind tunnel test report. The modal data from the finite element model is extracted and used for the computational fluid dynamic analysis inside VXflow solver. The thesis proves the reasonably match result for free standing vertical tower between wind tunnel test of reference structure and result of numerical solver of VXflow, which has only averagely 10% differences in peak displacement of three erection stages and succeed to predict strouhal number with 10% difference.

The tuned mass damper then added inside the numerical software VXflow in terms of effective damping. The parameter of tuned mass damper taken from Den Hartog's optimum damping and optimum frequency ratio. The effective damping reached $\zeta_d = 0.163$. The result shows, the peak displacement reduced by average of 67%. This shows the effectiveness of TMD for reducing peak displacement due to vortex induced vibration.

Uncoupled analysis is later done by taking aeroelastic loads from VXflow then applied inside the finite element model and obtain the responses. It is uncoupled because the interaction between wind and structure due to this aeroelastic phenomena could not be captured inside the finite element software. However, the detailed responses such as internal forces, acceleration, and TMD displacement due to aeroelastic loads can be observed in more straightforward manner. The freestanding vertical model without TMD is reasonably agrees with VXflow simulation, with average discrepancy of 25%. Then the finite element model with TMD is simulated and the reduction of this model with respect to model without TMD reaches averagely 76%. The reduction rate due to TMD has 15% difference between coupled and uncoupled method.

The comparison about using single and multiple TMD is also done, and both of TMD has reduced in the same level rate around 69% acceleration response.

According to Moon [18], tuned mass damper will give more benefit if installed as multiple distributed tuned mass dampers along the height instead of one single TMD at top of structure. The benefits are regarding the space, installation, construction, and reliability. But the placement of multiple TMD has never been observed, so that parametric simulation of TMD distribution is performed. The result shows that the

TMD that distributed with polynomial spacing gives 7.8% better result than the one that distributed with equal spacing.

Mass ratio of TMD is also crucial to determined because the construction cost will highly depend on this. A parametric simulation has done, and found out that the optimum mass ratio achieved with 1.25% of mass of predominant frequency.

5.3 Recommendation for Future Work

Recommendations which could be done for future works are as follows:

- VXflow simulations can achieve more accurate results by increasing number of time steps, increasing number of panels, however it requires longer computational time.
- Finding better agreement from comparison of uncoupled and coupled analysis. This is done by having more exact numerical models and accurate modal data.
- Run the parametric simulation inside CFD environment, to receive better coupled responses.

REFERENCES

- [1] Balendra, T. *Vibration of Buildings To Wind And Earthquake Loads*. Springer Verlag, Singapore, 1993.
- [2] Pedley, T. J. *Introduction to Fluid Dynamics*. Journal of Scientia Marina, Department of Applied Mathematics and Theoretical Physics, University of Cambridge, 1997.
- [3] Simiu, E. Scanlan, R.H. *Wind Effects on Structures, 3rd Edition*. John Wiley & Sons, Inc., New York, 1996.
- [4] BMT Fluid Mechanics Limited. *Stonecutters Bridge Full Aeroelastic Freestanding Tower Wind Tunnel Testing*. Middlesex, June 2005.
- [5] Milani, D., Morgenthal, G. *Temporal and Spatial Adaptation in Aerodynamic Simulation of Bluff Bodies Using Vortex Particle Methods*. Bauhaus University Weimar, Weimar, 2015.
- [6] Morgenthal, G. *VX Flow Primer v.0995*. Bauhaus University Weimar, Weimar, 2013.
- [7] Kiviluoma, Risto. *Frequency-domain approach for calculating wind-induced vibration and aeroelastic stability characteristics of long-span bridges*. Finnish Academy of Technology, Helsinki, 2001.
- [8] Davenport, A.G. *What makes a structure wind sensitive?* Boundary Layer Wind Tunnel Laboratory, The University of Western Ontario, London, Ont., Canada, 1998.
- [9] Niemann, H.-J. and Hölischer, N. *A Review of Recent Experiments On The Flow Past Circular Cylinders*. Building Aerodynamics Laboratory, Ruhr-Universität Bochum, Bochum (F.R.G.), 1990.
- [10] Schewe, G. *On the force fluctuations acting in circular cylinder in cross flow from subcritical up to transcritical Reynolds numbers*, Vol. 133, pp.265-285, 1983.
- [11] Morgenthal, G., Sham, R., West, B. *Engineering the Tower and Main Span Construction of Stonecutters Bridge*. Journal of Bridge Engineering, ASCE, pp.144-152, March/April 2010.
- [12] SOFiSTiK AG. *SOFiSTiK DYNA Dynamic Analysis Version 13.01*. Oberschleisheim, 2011.
- [13] Zabel, Volkmar. *Structural Dynamics Winter Semester 2013/14*. Institut für Strukturmechanik, Bauhaus Universität Weimar, Weimar, 2013.
- [14] Buresti, G. *Vortex Shedding From Bluff Bodies*. Journal of Wind Effects on Building and Structures, Riera & Davenport, Balkema, Rotterdam, pp 61-95, 1998.
- [15] Goswami, I., Scanlan, R. H., and Jones, N. P. *Vortex-Induced Vibrations of Circular Cylinders. I: Experimental Data; II: New Model*. Journal Engineering Mechanics 119, pp 2270-2303, 1993.

- [16] Frahm, H. *Device for damping vibration of bodies*. US Patent 989958, 1909.
- [17] IEEE Instrumentation and Measurement Society. *IEEE Standard on Transitions, Pulses, and Related Waveforms*. New York, 2003.
- [18] Moon, K. Y. *Vertically Distributed Multiple Tuned Mass Damper in Tall Buildings: Performance Analysis and Preliminary Design*. The Structural Design of Tall and Special Buildings vol. 19, pp 347-366, 2010.
- [19] Yang, J. N., Agrawal A. K., Samali, B. *A Benchmark Problem for Response Control of Wind-Excited Tall Buildings*. Journal of Engineering Mechanincs, vol. 130, no. 4, pp. 437-446, 2004.
- [20] Elias, S. Matsagar, V. *Distributed Multiple Tuned Mass Dampers for Wind Vibration Response Control of High-Rise Building*. Journal of Engineering, Hindawi Publishing Corporation, 2014.
- [21] Yang, F., Sedaghati, R., and Esmailzadeh, E. *Optimal design of distributed tuned mass dampers for passive vibration control of structures*. Journal Structural Control and Health Monitoring, vol 22, pp 221-236, 2015.
- [22] Vejrum, T., Bergman, D. W., Yeung, N. *Stonecutters Bridge, Hong Kong: Design and construction of the composite upper tower in stainless steel*. 2009.
- [23] Wang, H., Tao, T., Cheng, H., Li, A. *A simulation study on the optimal control of buffeting displacement with multiple tuned mass dampers*. Journal of Zhejiang University-SCIENCE A, 2014.
- [24] Brar, J.S., Bansal, R.K. *A Text Book of Theory of Machines*. Laxmi Publication, New Delhi, 2004.
- [25] Haselbach, P., Natarajan, A., Jiwinangun, R. G., Branner, K. *Comparison of coupled and uncoupled load simulations on a jacket support structure*. 10th Deep Sea Offshore Wind R & D Conference, DeepWind, 2013.

APPENDICES

Appendix A

Input for VXflow

NSLICES=6

U0X=9.5
VISCTY=0.000015
DIFFU=1
DELTAT=1.0
NSTEPS=15000

SUBSTEP=1
NPANELFACT=1
FASTMODE=2
TINTEGR=1
SURF=2
INSIDE=2
CROSS=0
COREMODEL=2
DYNAMIC=1
STRCMODEL=4
MODEFILE=modes.txt
SLICEFILE=slices.txt
NR=3

WINMINX=-40
WINMAXX=260
WINMINY=-75
WINMAXY=75
RSTFL=0

VXFL=0
VXSTEP=10
VIZFL=0
FVFL=0
FVSTEP=10

ISOMINX=-20
ISOMAXX=100
ISOMINY=-30
ISOMAXY=30
ISODIMX=200
ISODIMY=100
!NMDELTA=0.5
!NMBETA=0.5
!!

NUMSEC=1
!NUMSEPSEC=1
ASEC0=322.58
GEOMROT=0.0
ROTCENTREX=0.0
ROTCENTREY=0.0
CORER=1.2
AVGPRESS=1
GRIDMINX=-40
GRIDMAXX=260
GRIDNX=511
GRIDMINY=-75
GRIDMAXY=75
GRIDNY=255

!!

4//num_cornerpoints
0.2 0.0 //release_distance*spacing_hull
0.02 0.001 0.0 -0.1 //merg1*merg2*merg3*merg4
-4 -3 -1 -3 -1 //section_color_coding:drag*lift*moment*displ*rotation
1.000000e+00 -8.665000e+00 2.500000e+00 1.000000e+01
2.000000e+00 -8.665000e+00 -2.500000e+00 5.400000e+01 0 -2.500000e+00
1.000000e+00 8.665000e+00 -2.500000e+00 1.000000e+01
2.000000e+00 8.665000e+00 2.500000e+00 5.400000e+01 0 2.500000e+00

!2

NUMSEC=1
!NUMSEPSEC=1
ASEC0=153.94
GEOMROT=0.0
ROTCENTREX=0.0
ROTCENTREY=0.0
CORER=1.2
AVGPRESS=1
GRIDMINX=-40
GRIDMAXX=260
GRIDNX=511
GRIDMINY=-75
GRIDMAXY=75
GRIDNY=255

```
!!
2//num_cornerpoints
0.2 0.0 //release_distance*spacing_hull
0.02 0.001 0.0 -0.1 //merg1*merg2*merg3*merg4
-4 -3 -1 -3 -1 //section_color_coding:drag*lift*moment*displ*rotation
2 -7 0 44 0 0
2 7 0 44 0 0
```

```
!3
NUMSEC=1
!NUMSEPSEC=1
ASEC0=123.35
GEOMROT=0.0
ROTCENTREX=0.0
ROTCENTREY=0.0
CORER=1.2
AVGPRESS=1
GRIDMINX=-40
GRIDMAXX=260
GRIDNX=511
GRIDMINY=-75
GRIDMAXY=75
GRIDNY=255
```

```
!!
```

```
2//num_cornerpoints
0.2 0.0 //release_distance*spacing_hull
0.02 0.001 0.0 -0.1 //merg1*merg2*merg3*merg4
-4 -3 -1 -3 -1 //section_color_coding:drag*lift*moment*displ*rotation
2 -6.27 0 39 0 0
2 6.27 0 39 0 0
```

```
!4
NUMSEC=1
!NUMSEPSEC=1
ASEC0=93.31
GEOMROT=0.0
ROTCENTREX=0.0
ROTCENTREY=0.0
CORER=1.2
AVGPRESS=1
```

```
GRIDMINX=-40
GRIDMAXX=260
GRIDNX=511
```

GRIDMINY=-75
GRIDMAXY=75
GRIDNY=255

!!

2//num_cornerpoints
0.2 0.0 //release_distance*spacing_hull
0.02 0.001 0.0 -0.1 //merg1*merg2*merg3*merg4
-4 -3 -1 -3 -1 //section_color_coding:drag*lift*moment*displ*rotation
2 -5.45 0 34 0 0
2 5.45 0 34 0 0
!5
NUMSEC=1
!NUMSEPSEC=1
ASEC0=67.25
GEOMROT=0.0
ROTCENTREX=0.0
ROTCENTREY=0.0
CORER=1.2
AVGPRESS=1
GRIDMINX=-40
GRIDMAXX=260
GRIDNX=511
GRIDMINY=-75
GRIDMAXY=75
GRIDNY=255

!!

2//num_cornerpoints
0.2 0.0 //release_distance*spacing_hull
0.02 0.001 0.0 -0.1 //merg1*merg2*merg3*merg4
-4 -3 -1 -3 -1 //section_color_coding:drag*lift*moment*displ*rotation
2 -4.63 0 34 0 0
2 4.63 0 34 0 0

!6

NUMSEC=1
!NUMSEPSEC=1
ASEC0=46.35
GEOMROT=0.0
ROTCENTREX=0.0
ROTCENTREY=0.0
CORER=1.2
AVGPRESS=1


```
GRIDMINX=-40
GRIDMAXX=260
GRIDNX=511
GRIDMINY=-75
GRIDMAXY=75
GRIDNY=255
```

```
!!
```

```
2//num_cornerpoints
0.2 0.0 //release_distance*spacing_hull
0.02 0.001 0.0 -0.1 //merg1*merg2*merg3*merg4
-4 -3 -1 -3 -1 //section_color_coding:drag*lift*moment*displ*rotation
2 -3.85 0 24 0 0
2 3.85 0 24 0 0
```

Appendix B

Sofistik Code for TMD Calculation

```
+PROG AQUA urs:1
HEAD Materials+Section
NORM EC 2
PAGE UNII 0 $Units in m
ECHO FULL
$Material Definition
CONC NO 1 TYPE C 30 GAM 35
STEE NO 2 TYPE S 500
CONC NO 3 TYPE C 40 GAM 30
STEE NO 4 TYPE S 420M
$Creating loop for section 5-5
LOOP#1 30
SECT NO 10+#1 MNO 1 MRF 2
POLY TYPE OPZ
VERT NO Y Z R PHI TYPE
1 0 9-#1*0.0667
2 -3.0+#1*0.1 9-#1*0.0667
3 -3.0+#1*0.1 -9+#1*0.0667 9.0-#1*0.0667 10 O
4 0 -9+#1*0.0667
POLY TYPE OPZ MNO 0
VERT 5 0 7-#1*0.0667
6 -3.0+#1*0.1 7-#1*0.0667
7 -3.0+#1*0.1 -7+#1*0.0667 7.0-#1*0.0667 10 O
8 0 -7+#1*0.0667
CUT 1 ZB S
ENDLOOP
$FULL SECT 4-4
SECT NO 100 MNO 1 MRF 2
POLY TYPE OPZ
VERT NO Y Z R PHI TYPE
1 0 7
2 0 -7 7 10 O
CUT 1 ZB S
LOOP#3 40
SECT NO 101+#3 MNO 1 MRF 2
POLY TYPE OPZ
VERT NO Y Z R PHI TYPE
1 0 7-#3*0.0386
2 0 -7+#3*0.0386 7-#3*0.0386 10 O
```

```

POLY TYPE OPZ MNO 0
VERT NO Y Z R PHI TYPE
3 0 5-#3*0.0236
4 0 -5+#3*0.0236 5-#3*0.0236 10 O
CUT 1 ZB S
ENDLOOP
LOOP#5 51
SECT NO 200+#5 MNO 3 MRF 2
POLY TYPE OPZ
VERT NO Y Z R PHI TYPE
1 0 5.45-#5*0.03741
2 0 -5.45+#5*0.03741 5.45-#5*0.03741 10 O
POLY TYPE OPZ MNO 0
VERT NO Y Z R PHI TYPE
3 0 5.45-#5*0.03741-1.4+#5*0.0086
4 0 -(5.45-#5*0.03741-1.4+#5*0.0086) 5.45-#5*0.03741-1.4+#5*0.0086
10 O
CUT 1 ZB S
ENDLOOP
SCIT NO 301 D 7 T 0.02 MNO 4
END

```

```

+PROG SOFIMSHA urs:2
Head Stonecutter Geometry
PAGE UNII 0 ; syst SPAC
GRP 1

```

```

NODE (10 40 1) X 0 Y 0 Z (-2.20 -2.52)
NODE (41 81 1) X 0 Y 0 Z (-80.23 -2.43)
NODE (82 132 1) X 0 Y 0 Z (-177.59 -2.36)
NODE (133 134 1) X 0 Y 0 Z (-297.7 -2.5)
NODE 10 0 0 -2.20 fix f
$NODE 200 X 0.2 Y 0 Z -32.44 fix XP $Additional Node for damper
NODE 201 X 0.2 Y 0 Z -62.68 fix XP
$NODE 202 X 0.2 Y 0 Z -92.38 fix XP
NODE 203 X 0.2 Y 0 Z -119.110 fix XP $Additional Node for damper
$NODE 204 X 0.2 Y 0 Z -148.270 fix XP
NODE 205 X 0.2 Y 0 Z -177.43 fix XP
$NODE 206 X 0.2 Y 0 Z -208.276 fix XP $Additional Node for damper
NODE 207 X 0.2 Y 0 Z -236.59 fix XP
NODE 209 X 0.2 Y 0 Z -295.590 fix XP $Additional Node for damper
$Beam Definition from +2.2 until +77.75
LOOP#2 30
BEAM NO #2+1 NA #2+10 NE #2+11 NCS 10+#2
ENDLOOP
$Intermediate full crosssection 4-4
BEAM NO 100 NA 40 NE 41 NCS 100
LOOP#4 40
BEAM NO 101+#4 NA 41+#4 NE #4+42 NCS 101+#4
ENDLOOP
LOOP#6 51
BEAM NO 200+#6 NA 81+#6 NE 82+#6 NCS 200+#6
ENDLOOP
$LOOP#7 2
$BEAM NO 300+#7 NA 132+#7 NE 133+#7 NCS 301
$ENDLOOP

```

```

#define stiffness=33.27
#define mass=29.81
#define damping=3.78
$ SPRI NO 1 NA 22 NE 200 CP 37 DP 2
SPRI NO 2 NA 34 NE 201 CP $(stiffness) DP $(damping)
$ SPRI NO 3 NA 46 NE 202 CP 37 DP 2
SPRI NO 4 NA 57 NE 203 CP $(stiffness) DP $(damping)
$ SPRI NO 5 NA 69 NE 204 CP 37 DP 2
SPRI NO 6 NA 81 NE 205 CP $(stiffness) DP $(damping)
$ SPRI NO 7 NA 95 NE 206 CP 37 DP 2
SPRI NO 8 NA 107 NE 207 CP $(stiffness) DP $(damping)
$ SPRI NO 9 NA 119 NE 208 CP 37 DP 2
SPRI NO 10 NA 132 NE 209 CP $(stiffness) DP $(damping)
MASS NO (201 209 2) MX $(mass)
END

+PROG SOFILOAD urs:3
HEAD Wind Lift Time History Forces
ECHO FUNC EXTR
LC 10; NODE NO 132 TYPE PXX 1.0;
FUNC 0.00 0
0.1 10000
FUNC F
0;0
#define dt1=0.2
#define N1=3600
STEP N $(N1) DT $(dt1) LCST 101 $ vgl. step_sofiloader.dat
$ comp

END

-PROG SOFILOAD urs:4
HEAD Wind Lift Time History Forces
ECHO FUNC EXTR
LC 10; NODE NO 20 TYPE PXX 0.001;
FUNC 0.00 0
2.412011e-001 0
FUNC F
352.78;10.548;1142.9;-613.85;1385.2
STEP N $(N1) DT $(dt1) LCST 101 $ vgl. step_sofiloader.dat
$ comp
END
+PROG ASE urs:11
HEAD Time History Iteration
STEP N $(N1) DT $(dt1) THE 0.7
GRP 0,1,2,3,4,5,6,7,8,9 RADA 0.0009 RADB 0.001
LC 101
$HIST NODE FROM 3 TO 4
ECHO DISP YES
END $ -j see ASE-Graphik-Plot or node 1 vx in dbview graphically
!

+PROG ASE URS:13
HEAD Verformungsplot $ deformation curve

```

PLOT LC 101 NNO 132 DIRE X TYPE TIME
PLOT LC 101 NNO 132 DIRE AX TYPE TIME
END

+PROG DBPRIN urs:18
HEAD OUTPUT TIME HISTORY
CTRL WARN 900
PAGE 1 UNIO 7
ITEM TYPE NODE KIND DISP
ITEM TYPE NODE KIND ACCE
SELE NO 132
PRIN SORT ELEM
ECHO RES YES
END

+PROG DBPRIN urs:5
HEAD OUTPUT MAXIMUM and MINIMUM
CTRL WARN 900
PAGE 1 UNIO 7
ITEM TYPE NODE KIND DISP
ITEM TYPE NODE KIND ACCE
SELE NO 132
PRIN RANG MAMI
ECHO RES YES
END